Synthesis and characterization of functionalized 2° amines 2-(alkylamino)-3-chloro-1,4-naphthoquinones: Effect of *N*-substituents on crystal packings, fluorescence, redox and anti-microbial properties

Abstract

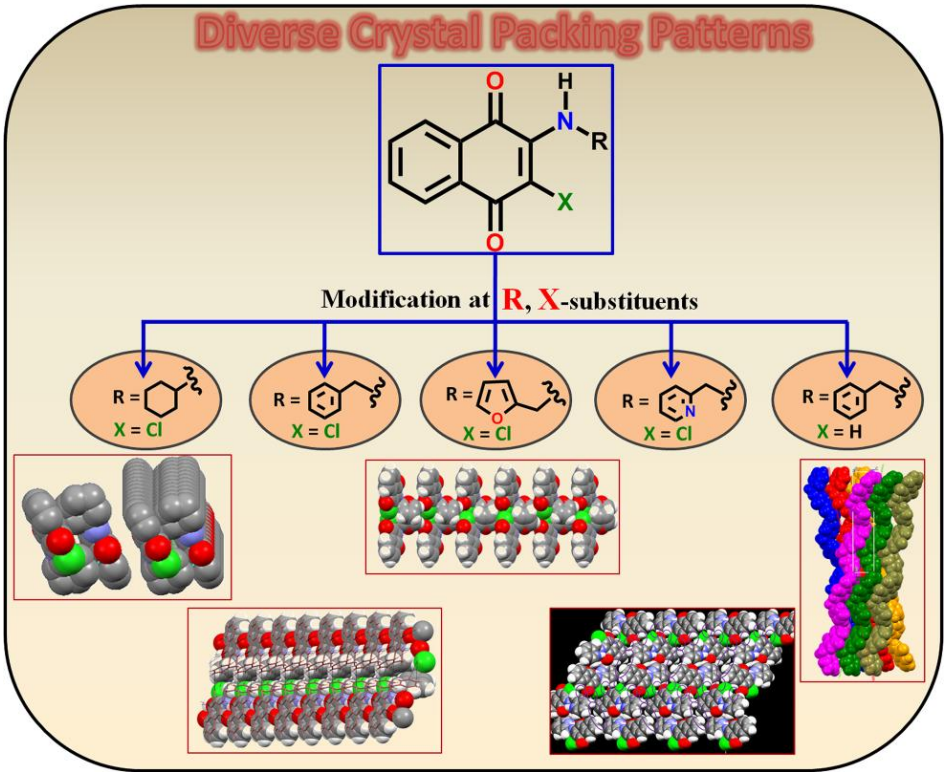

Chemo-selective reaction of 2, 3-dichloro-1,4-naphthoquinone with different primary amines affords access to a series of derivatives such as 2-(alkylamino)-3-chloro-1,4-naphthoquinone (**1-6**) and 2-(benzylamino)-1,4-naphthoquinone (**7**) in good yields. All the compounds **1-7** have been characterized thoroughly by microanalysis, standard spectroscopy and thermogravimetric method. Supramolecular structures of **1–4** and **7** have been studied by means of single-crystal X-ray diffraction to gauge the influence of substituents, present on amine functionality, on the association of molecules in the solid state. The study showed that the introduction of various amine *N*-substituents induces conformational changes that apparently modify the nature and number of donor-acceptor sites for noncovalent interactions, leading to diverse crystal packing patterns. Interestingly, the introduction of 2-(benzylamino)- and 2-(2-pyridylmethylamino)- substituents in **2** and **4**; successfully switches on C-Cl...π synthon, scarcely seen in the crystal packing of organic molecules. Compounds

1, 2, 4 and **5** fluoresces in the range of 350-620 nm with concomitant Stoke shifts of 81, 131, 141 and 131 nm, respectively and their cyclic voltammograms evidence two quasi-reversible single-electron waves. All the compounds (except **5**) exhibit first endothermic peak on the DTA curves without any mass loss due to the phase change attributable to the melting points of respective compounds. Remarkably, compound **5** exhibits enhanced antibacterial activity against S. Aureus and proved to be more potent antibacterial agent than a well known drug "ciprofloxacin".

4A.1. Introduction

The intermolecular forces that hold the molecules in the solid state are inadequately understood and hard to predict, particularly for organic solids [1]. Since the material's properties are often governed by the way in which their constituent molecules are arranged, [2] any step taken into predictable molecular packing is a practical movement towards the ultimate goal of structural chemistry to design new solid of desired properties. The hydrogen bonds and stacking interactions including weak hydrogen bonds like C–H…O, [3] N–H…O, [4] C–H…π [5] and π…π [6] interactions were considered as main directing tool in the organization of molecules in both chemistry as well as in biology. These were implicated successfully in the crystal engineering and supramolecular assemblies. However, the ability of halogen atoms to function as reliable sites for directing intermolecular recognition processes was largely overlooked until the 1990s. The halogen bonds have been recognized recently as another type of non-covalent interactions that can be used as a new tool for the organization of supramolecular systems and molecular crystals [7]. They have been shown to be accountable for the formation of a variety of stable supramolecular assemblies in crystals, [7c,8] biological systems, [9] solutions, [10] and even in the gas phase [11]. A competition between hydrogen bonding and halogen bonding has been observed by Professor Aakeroy's group and others, [12] during supramolecular assembling of organic molecules in the solid state. Of more interesting, rational modifications of the hierarchy of intermolecular interactions in molecular crystal structures by using tuneable halogen bonds were developed [13]. In particular, halogen bond of the type C-H...Cl [7b,14] has been investigated significantly, however literature evidences a fewer report [8,15] on the existence of C-Cl…π interactions. A survey of the protein data bank (PDB) suggests only limited number of

C-Cl…π interactions, retrieved from crystal structures of protein–ligand complexes [15]. Thus, considerably larger data on C-Cl…π contacts should help us better evaluate the characteristics of such interactions in biomolecules and in structural chemistry.

Apart from this, considerable attention has been paid on the functionalization of naphthoquinone derivatives and evaluation of their biological properties, [16] mainly due to their association in multiple biological oxidative processes, [17] and thus have a great impact on the biological systems. A large part of the biological activity of quinonoid systems is shown to be related to its capacity to generate free radicals via redox reactions which involve electrogenerated radical anion species (semiquinone) with long half-life periods and able to transfer the electron to another species in vivo [18]. Reportedly, naphthoquinone derivatives possess diverse biological properties that include antibacterial and antifungal, [19] antiviral, [20] antimalarial [21] and anticancer [22] activity which have stimulated the study of these bioactive compounds in the field of medicinal chemistry.

This paper outlines a facile synthesis, spectral, optical and thermal characterization of 2-(alkylamino)-3-chloro-1,4-naphthoquinones **1-6** and 2-(benzylamino)-1,4-naphthoquinone **7** (Chart 1). The single crystal X-ray diffraction technique has been used to facilitate the understanding of structures and to review the influence of various *N*-substituents on the crystal packing patterns in the solid state. We have determined the crystal structure for five 2-substituted 3-chloro-1,4-naphthoquinone derivatives and have analyzed the propensity of the formation of C–Cl…π, C–H…Cl and C–H…π contacts in the presence of dominating C–H...O contacts and the directional preference in terms of crystal packing. These derivatives form an interesting class of compounds with synthetic versatility and effective anti-microbial activities. Due to the increasing importance of halogen bonding in biological systems, [16] the identification of C–Cl…π, C–H…Cl intermolecular interactions in **2** and **4** would add merit and assist the evaluation of the characteristics of such interactions in biomolecules and in structural chemistry.

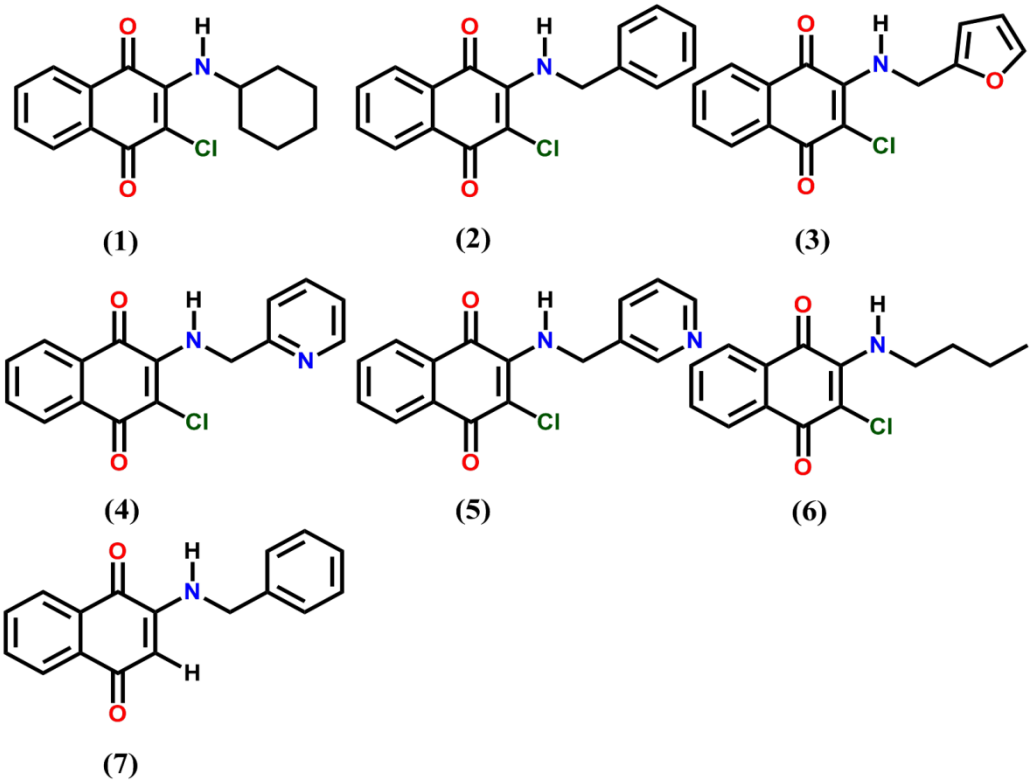

Chart 1: Compounds 1–7 under investigation.

4A.2. Results and discussion

4A.2.1. Synthesis and characterization

Chemo-selective reaction of 2, 3-dichloro-1,4-naphthoquinone with different primary amines efficiently yielded a series of novel 2-substituted-1,4-naphthoquinone derivatives such as 2-(alkylamino)-3-chloro-1,4-naphthoquinones (**1-6**) and 2-(benzylamino)-1,4-naphthoquinone (**7**) in good yields (Scheme 1). The dual roles of amine as nucleophile and as a base, facilitate the formation of products in EtOH *via* removal of one chloro substituent with ease. Remarkably, only the reaction of 2,3-dichloro-1,4-naphthoquinone with benzyl amine in refluxing DMF lead to the formation of 3-hydro analogue **7**. Compounds **2**, **6** and 7 have been synthesized by a modified literature procedures [23] and this modification was scalable to 95% for **2**, 90% for **6** and 70% in less time, unlike the original methods [23a,b,d].

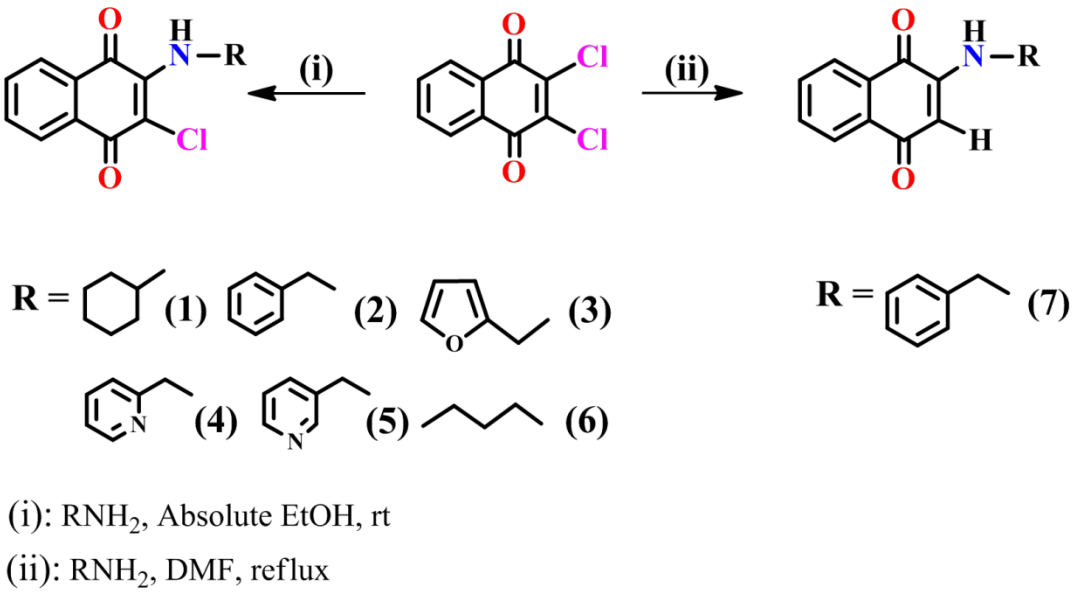

Scheme 1 Synthetic Protocol for 2-(alkylamino)-3-chloro-1,4-naphthoquinones **(1-6)** and 2-(benzylamino)-1,4-naphthoquinone **(7)**

All the compounds **1-7** have been characterized thoroughly by microanalysis, standard spectroscopy and thermogravimetric method. The spectroscopic analysis data, such as GC-MS, IR, NMR and UV-visible spectra of the compounds **1-7** are consistent with their chemical formula determined by elemental analysis and the structures of **1-4** and 7 were elucidated from single crystal X-ray diffraction study.

In the IR spectra of **1-7**, the most characteristic bands observed between 3250–3350 cm^{-1} are diagnostic of υ(N-H) stretching vibrations. The weak intensity bands appeared in the regions of 3147-2931 cm^{-1} are attributable to the aromatic υ(C-H) stretching vibrations, whereas bands appeared in the regions of 850-820 cm^{-1} are assignable to the aromatic υ(C-H) out-of plane bending vibrations, a characteristic feature of phenyl ring of naphthoquinone moiety. Additionally, **1-7** display strong bands (1675–1683 cm^{-1}) and medium intensity bands (1140-1124 cm^{-1}) due to υ(C=O) and υ(C-N) vibrations [24]. Unlike **7**, compounds **1-6** display a sharp band in the region of 719-725 cm^{-1} due to υ(C-Cl) stretching vibrations. The ^{1}H NMR spectra of **1-7**, exhibit most characteristic signals in the range of δ = 6.10-7.82 ppm due to amine –NH moiety along with signals due to aromatic protons of naphthoquinone moiety and corresponding *N*-substituent with proper splitting pattern. Among these, –NH signal in compound **4** is significant downfield shifted due to higher electron withdrawing nature of *N*-(2-pyridylmethyl) substituent. A singlet signal appeared at δ

= 5.82 ppm is assignable to the proton present at 3-position of 2- (benzylamino)-1,4-naphthoquinone **(7**). In ^{13}C spectra of **1-7**, the most characteristic signals appeared in the range of δ = 181–176 ppm is attributable to the two quinonic carbonyl moieties. Compound **1** displays singals due to methine and methylene groups at 52.5 ppm and δ = 35-24 ppm regions, respectively. In case of compound **2-5**, signal in the range of 41–49 ppm are assigned to methylene carbon atoms whereas signals observed in δ = 155–108 ppm regions are due to aromatic carbons. Compound **6**, shows three upfield signals in δ = 44-19 ppm regions due to $–CH_2$ while a signal appeared at δ = 13.7 ppm corresponds to $–CH_3$ moiety of n-butyl substituent. The IR, ^1H and ^{13}C NMR spectral data for **1-7** are consistent with similar compounds reported in the literature. Compounds **1**, **2, 4** and **7** were further characterized by mass spectroscopy. The molecular ion peak (m/z) corresponds to = (M+H) and gives the evidence for the formation of the desired compounds.

Block shaped colourless crystals for **1**, **2**, **4** and golden-yellow crystals for compound **3**, suitable for single crystal X-ray diffraction study, were grown from dichloromethane solution by slow evaporation at 4 °C. Our efforts to obtain single crystals of **5** and **6** suitable for XRD analysis using different crystallization techniques were unsuccessful. The crystal data and structure refinement for compounds **1-4** and **7** are given in Table 1.

Table 1 Crystal data and structure refinement for compounds **1-4** and **7**

Identification code	**1**	**2**	**3**	**4**	**7**
Formula	$C_{16}H_{16}ClNO_2$	$C_{17}H_{12}ClNO_2$	$C_{15}H_{10}ClNO_3$	$C_{16}H_{11}ClN_2O_2$	$C_{17}H_{13}NO_2$
Formula weight	289.75	297.73	287.69	298.72	263.30
Temperature (K)	150(2)	293(2)	150(2)	150(2)	293
Wavelength (Å)	0.71073	0.71073	0.71073	0.71073	0.71073
Crystal system	Triclinic	Monoclinic	Monoclinic	Monoclinic	orthorhombic
space group	P -1	P 21/c	P 21/c	P 21/n	$Pna2_1$
a(Å)	8.1167(10)	10.2681(4)	7.4914(2)	5.0576(4)	10.8597(13)
b(Å)	8.3589(10)	7.7447(3)	20.7986(5)	11.4615(7)	24.115(4)
c(Å)	10.5321(13)	17.5818(9)	7.9056(2)	23.3465(11)	5.0303(7)
α(°)	92.178(10)	90	90	90	90
β(°)	104.565(11)	93.836(4)	93.019(2)	91.898(6)	90
γ(°)	94.094(10)	90	90	90	90
Volume($Å^3$)	688.68(15)	1395.03(10)	1230.07(5)	1352.60(15)	1317.3(3)
Z	2	4	4	4	4
Calculated density(mg/m^3)	1.397	1.418	1.553	1.467	1.3275
Absorption coefficient (m/mm^{-1})	0.278	0.277	0.317	0.288	0.088
F(000)	304	616	592	616	52.3
Crystal size (mm^3)	0.23 x 0.18 x 0.13	0.32 x 0.27 x 0.23	0.23 x 0.18 x 0.13	0.23 x 0.17 x 0.13	0.14 × 0.11 × 0.06
θ range for data collection (°)	3.07 to 25.00 deg.	2.95 to 25.00 deg.	3.24 to 25.00 deg.	3.17 to 24.99 deg.	6.76 to 55.84°
Index ranges	-9<=h<=9, -9<=k<=9, -12<=l<=12	-11<=h<=12, -5<=k<=9, -20<=l<=20	-8<=h<=8, -24<=k<=21, -9<=l<=9	-6<=h<=5, -13<=k<=13, -27<=l<=27	$-13 \le h \le 5$, $-31 \le k \le 28$, $-6 \le l \le 3$
Reflections collected / unique	5112 / 2429 [R(int) = 0.0424]	10267 / 2451 [R(int) = 0.0451]	8482 / 2164 [R(int) = 0.0165]	8228 / 2368 [R(int) = 0.0779]	1366 [R(int) =0.0306]
Completeness to theta = 25.00 (%)	99.8	99.9	99.8	99.9	99.9
Data / restraints / parameters	2429 / 0 / 181	2451 / 0 / 194	2164 / 0 / 181	2368 / 0 / 191	1366/0/181
Goodness-of-fit on F^2	1.036	1.004	1.082	1.120	1.118
Final R indices [I>2sigma(I)]	R1 = 0.0637, wR2 = 0.1655	R1 = 0.0441, wR2 = 0.1085	R1 = 0.0295, wR2 = 0.0707	R1 = 0.0652, wR2 = 0.1740	R_1 = 0.0718, wR_2 = 0.1410
Largest diff. peak and hole/ e $Å^{-3}$	0.335 and -0.387	0.210 and -0.233	0.299 and -0.265	0.445 and -0.672	0.28 and -0.33

Table 2 Significant intermolecular interactions [Interatomic distances (Å), and bond angles (°)] found in compounds **1-4** and **7**

Compounds	D─H…A	D─H	H…A	D…A	<DHA (β)	<α
1	C_{13}─H_{13a}…O1	0.970	2.709	3.471	135.81	…
	C_{12}─H_{12b}…O2	0.970	2.716	3.628	155.96	
	C_{16}─H_{16b}…O2	0.970	2.481	3.383	154.61	
2	C_6─H_6…O_1	0.930	2.303	3.218	168.61	…
	N_1─H_1N…O_2	0.862	2.295	3.051	146.38	
	C_{17}─H_{17}…O_2	0.930	2.715	3.533	147.26	
	C_9─Cl_1… C_g [Cg: C16 C17 C12 C13 C14 C15]	1.732	3.879	5.545	160.96	31.10
3	N_1─H_1…O_1	0.860	2.279	2.988	139.93	…
	C_{11}─H_{11}…O_2	0.970	2.570	3.356	138.19	
	C_{15}─H_{15}…O_2	0.930	2.572	3.331	139.13	
	C_{14}─H_{14}…O_2	0.930	2.601	3.507	164.89	
	C_{15}─H_{15}…Cl_1	0.930	2.916	3.472	119.69	
4	C_4─H_4…O_1	0.951	2.715	3.309	148.56	…
	C_6─H_{6B}…O_1	0.990	2.460	3.400	126.66	
	C_2─H_{2A}…O_2	0.951	2.593	3.302	131.58	
	C_8─Cl_1… C_{g1} [Cg1: C10C11 C12 C13 C14 C15]	1.736	3.768	5.468	165.87	6.15
	C_6─ H_{6A}… C_{g2} [Cg2: C7 C8 C9 C10 C15 C16]	0.991	3.472	3.808	102.30	21.2
	C_6─H_{6B}… C_{g3} [Cg3: C1 N1 C2 C3 C4 C5]	0.990	3.039	3.668	122.53	3.03
7	C_2─H_2…O_1	0.930	2.443	3.321	157.32	…
	N_1─H_1…O_2	0.860	2.168	2.901	143.03	
	C_{13}─H_{13}…O_2	0.929	2.709	3.511	144.98	
	C_{16}─ H_{16}… C_{g1} [Cg1: C4 C5 C6 C7 C8 C9]	0.930	2.522	4.407	159.94	36.36
	C_{11}─ H_{11b}… C_{g3} [Cg2: C1 C2 C3 C4 C9 C10]	0.970	3.480	4.280	143.62	11.66
	C_{g1}…C_{g2} [Cg3: C12 C13 C14 C15 C16 C17]	…	4.187	…	…	…

4A.2.2. Structural descriptions

A careful analysis of single crystal X-ray diffraction data reveals that a change in the *N*-substituents in **1-4** and absence of chloro substituent in **7**, changes the electronic nature as well as stereochemical conformations of the molecules. This can be clearly visualized from the different dihedral angles between the least squares plane through the naphthoquinone rings and that of amine substituents. The 3-chloro-1,4-naphthoquinone moiety having extended conjugation hold the two naphthoquinone rings virtually planar. The angle between the least squares planes through benzene and quinone rings of naphthoquinones appeared in a range of 0.99-2.29° in **1-4** and **7**. However, the angle between the least squares planes passing through the quinone ring

and various *N*-substituent ring, falls in the range of 61.88°-88.04° in all the molecules (except **4**), attaining a '*gauche*' conformational mode. Notably, the absence of chloro substituent in **7** diminishes the n-π electrostatic repulsive interactions and this molecule is largely deviates from a stable '*gauche*' conformational mode, revealed by the dihedral angle (88.04°) between naphthoquinone ring and benzene ring of the *N*-benzyl substituent. Contrarily, the presence of *N*-(2-pyridylmethyl) substituent in **4** changes the dihedral angle between the planes of naphthoquinone ring and pyridine ring to 0.99° and thus induces coplanarity in the molecular framework. These conformational changes induced by various amine *N*-substituents in **1-4** and **7** apparently modify the nature and number of donor-acceptor sites for noncovalent interactions, leading to diverse crystal packing patterns. This generates a scope for the control and fine tuning of the supramolecular assembly arise due to non-covalent interactions in these molecules. The supramolecular architectures arise due to a number of weak noncovalent intermolecular interactions in **1-4** and **7**, can be described as follows.

4A.2.2.1. X-ray structure of 2-(cyclohexylamino)-3-chloro-1,4-naphthoquinone [$C_{16}H_{16}ClNO_2$] (1)

Compound **1** crystallizes in chiral triclinic *P-1* space group and the X-ray crystal structure show asymmetric unit contains full molecule of [$C_{16}H_{16}ClNO_2$] as shown in Fig. 1(a). There are two such molecules in the unit cell. The selected bond distances (Å) and bond angles (°) for **1** are: C1-C6 1.475(4), C1-O1 1.211(3), C1-C2 1.522(3), C4-C5 1.499(4), C4-O2 1.223(3), C2-C3 1.370(4), C3-Cl1 1.738(2), C2-N1 1.337(3), N1-C11 1.463(3) Å and C6-C1-O1 122.0(2), C2-C1-O1 119.0(2), C5-C4-O2 119.5(2), C3-C4-O2 122.6(3), C2-C3-Cl1 122.7(2), C1-C2-N1 110.5(2), C2-N1-C11 131.2(2)°, respectively. The structural parameters are found to be in the normal range and have a good agreement with those observed for the similar compounds [25]. Interestingly, **1** containing cyclohexyl substituent on amine functionality adopts a '*gauche*' conformation, predominantly stabilized *via* a number of intermolecular CH...O interactions. The cyclohexyl group is primarily behaves as C-H donor and quinone group as C-H acceptor. Molecules of **1** are interconnected along *a*-axis in *anti* fashion through a number of CH...O interactions *viz.* C13-H13A...O1 (2.709 Å), C12-H12B...O2 (2.716 Å) and C16-H16B...O2 (2.481 Å) donor-acceptor interactions. In

fact one of the ketonic oxygen (O2) is involved in the bifurcated hydrogen bonding, arranging a molecule parallely and another molecule *anti*- parallely along *a*-axis. The relevant parameters for the weak interactions are tabulated in Table 2. The molecules present in the asymmetric unit forms a supramolecular unit, consists of five molecules aggregate, as shown in Fig. 1(b). Interestingly, these supramolecular units can be used to generate infinite network along *a*-axis, forming a fascinating 1D tubular architecture as shown in Fig. 1(c) and Fig. 1(d).

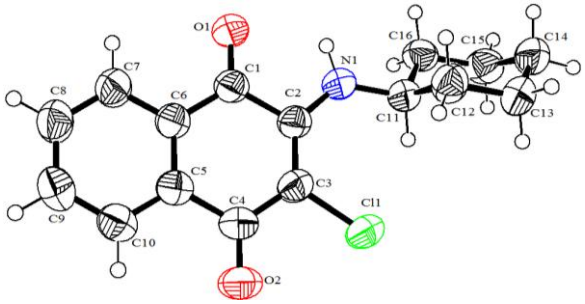

(a)

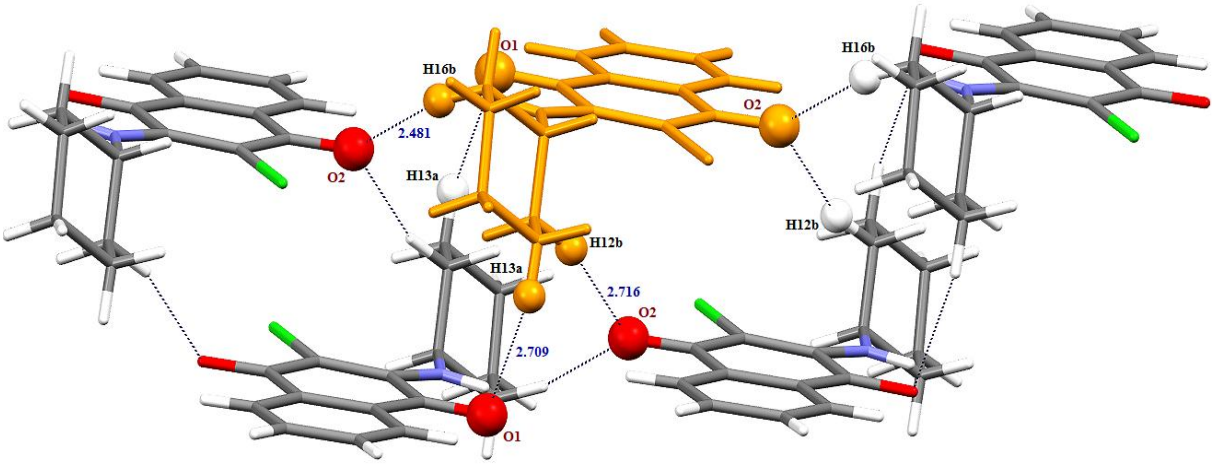

(b)

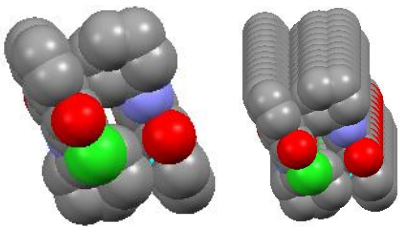

(c) (d)

Fig. 1 (a) Thermal ellipsoidal plot of compound **1** with atom labeling scheme; (b) Supramolecular unit consists of five molecule aggregates involving CH...O interactions; (c) Spacefill representation of molecular packing along *a*-axis forming 1D tubular architecture; (d) View of molecular packing in spacefill model along slightly tilted down from *a*-axis.

4A.2.2.2. X-ray structure of 2-(benzylamino)-3-chloro-1,4-naphthoquinone [$C_{17}H_{12}ClNO_2$] (2)

Compound **2** crystallizes in the centrosymmetric monoclinic P 21/c space group and the X-ray crystal structure show asymmetric unit contains full molecule of [$C_{17}H_{12}ClNO_2$] as shown in Fig. 2(a). There are four such molecules in the unit cell. The relevant parameters are tabulated in Table 1. The selected bond distance (Å) and bond angle (°) for **2** are: C1-C2 1.471(3), C1-O1 1.210(3), C1-C10 1.519(3), C7-C8 1.501(3), C8-O2 1.227(3), C8-C9 1.444(3), C9-Cl1 1.732(2), C10-N1 1.344(3), N1-C11 1.467(3), C11-C12 1.518(3) Å and C2-C1-O1 121.5(2), C10-C1-O1 119.1(2), C2-C1-Cl0 119.38(18), C7-C8-O2 119.6(2), C9-C8-O2 122.2(2), C7-C8-C9 118.16(18), C8-C9-C11 113.22(16), C10-C9-Cl1 122.83(18), C10-N1-Cl1 131.7(2), N1-C11-C12 112.56(17)°, respectively. These values followed the normal range and found consistent with similar type of compounds reported in the literature (*vide supra*). Notably, the presence of *N*-benzyl substituent efficiently changes the molecular orientation that has appeared to play a great role on crystal packing pattern of **2**. Molecules of **2** appeared to be involved in an unusual C-Cl...π donor-acceptor interactions (Fig. 2(b)) along with CH...O and N-H...O {C6-H6...O1 (2.303 Å), N1-H1...O2 (2.295 Å) and C17-H17...O2 (2.715 Å)} donor-acceptor interactions. It may be noted that similar to compound **1**, O2 is involved in the bifurcated CH...O interactions. The relevant parameters for weak interactions present in compound **2** are given in Table 2. Probably, the *anti*-parallel orientations of phenyl and naphthoquinone rings, adopting *'gauche'* conformation with dihedral angle of 72.79° is responsible for efficient C-Cl...π interactions. For such interactions to occur, it is not mandatory that the chlorine atom should be positioned directly above the phenyl ring plane with orthogonal orientation. Statistical data retrieved from PDB suggest that in majority cases of protein–ligand complexes, [15] the frequency distributions of α angle (angles between the vector along the Cg–Cl line and the normal to the plane of the ring) and β angle (∠ C–Cl–Cg º) as shown in Fig. 3, varies in the range of 20-30 º and160-180 º. Compound 2 display Cl...Cg distance (3.879 Å) and favourable α angle (31.10°) in the standard range [15,26]. The α angle was calculated from α = 90°-θ where θ is the angle of intersection of the phenyl ring plane (58.90°) and the β angle C9-Cl1···Cg (Cg: C16 C17 C12 C13 C14 C15) of 160.96° is adequately large to facilitate the effective C–Cl...π interactions. In solid state, the molecule present in the

asymmetric unit forms four donor-acceptor contacts viz. C6-H6$_{(naphthoquinone)}$...O1, N1-H1...O2, C17-H17$_{(benzylic)}$...O2 and C11-Cl11... $\pi_{(benzylic)}$ interactions that leads to a five molecules supramolecular aggregate as shown in Fig. 2(b). Notably, C-Cl...π donor-acceptor interactions efficiently managed the *anti* orientation of packed molecules limiting the growth of self-assembly along *c*-axis, however, the dimensionality has been extended along *b*-axis through C-H...O and N-H...O interactions leading to the fascinating 1D infinite supramolecular chair-like architecture as shown in Fig. 2(c) and Fig. 2(d).

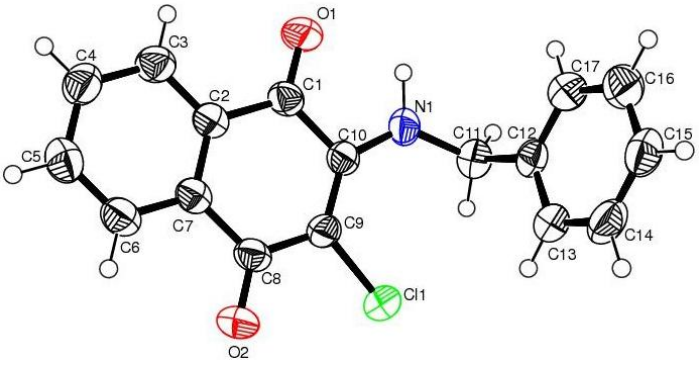

(a)

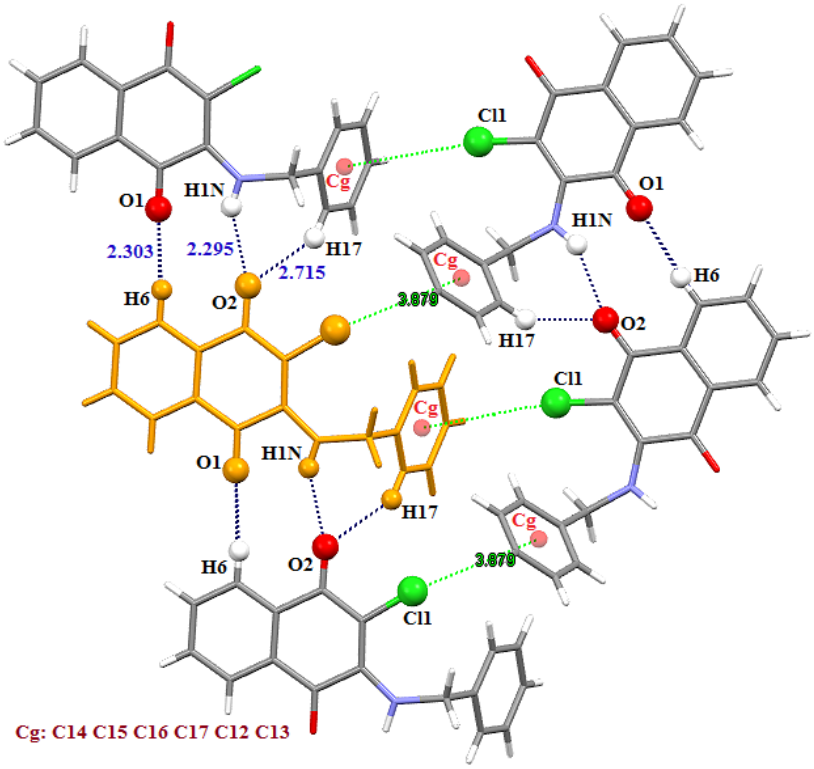

(b)

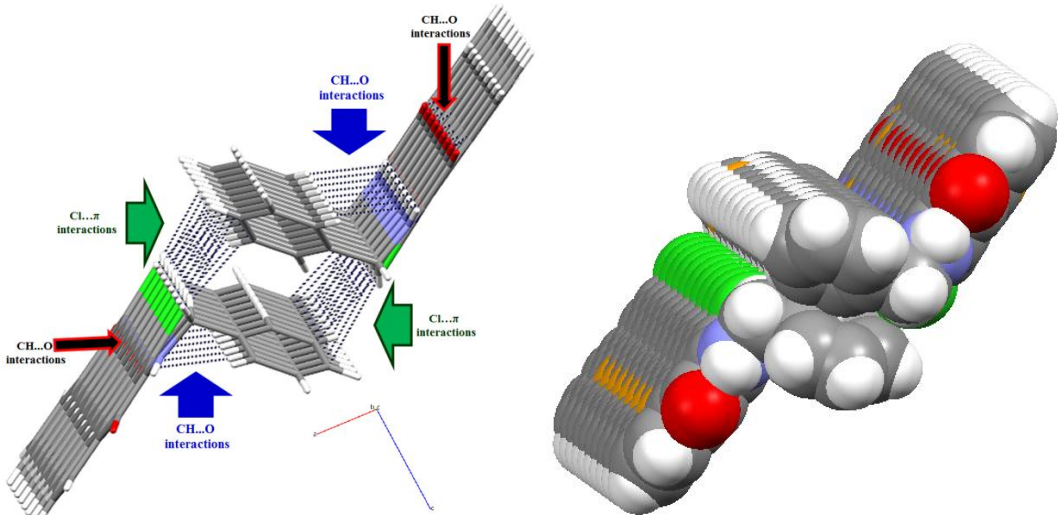

(c) (d)

Fig. 2 (a) Thermal ellipsoidal plot of compound **2** with atom labeling scheme (b) supramolecular unit consists of five molecule aggregates involving CH...O, NH…O and Cl…π interactions (c) Formation of 1D infinite supramolecular chair-like architecture (d) Spacefill representation of molecular packing along *b*-axis.

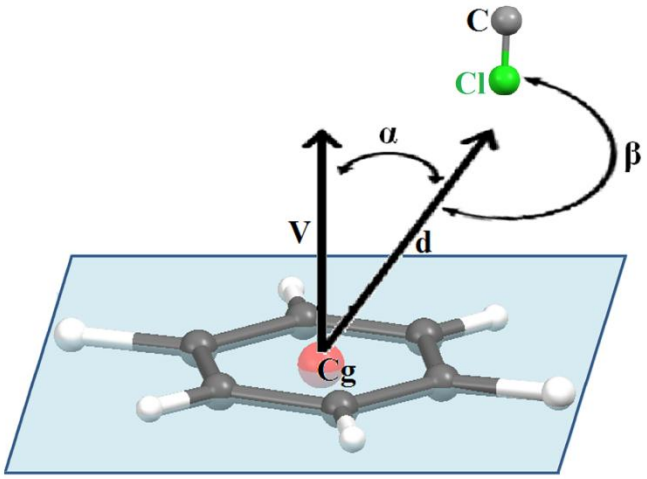

Fig. 3 Protocol for Cl...π interactions: d is the distance between the phenyl ring centroid (Cg) and the H atom; V is the vector normal to the plane of phenyl ring; α is the angle between the d and V vector, and β is the C–Cl...π angle.

4A.2.2.3. X-ray structure of 2-(furfurylamino)-3-chloro-1,4-naphthoquinone [$C_{15}H_{10}ClNO_3$] (3)

Compound **3** crystallizes in the centrosymmetric monoclinic P 21/c space group and the X-ray crystal structure show asymmetric unit contains full molecule of [$C_{15}H_{10}ClNO_3$] as shown in Fig. 4(a). Similar to the compound 2, there are four molecules in the unit cell. The relevant parameters are tabulated in Table 2. The selected bond distance (Å) and bond angle (°) for **3** are: C1-C2 1.454(2), C4-O1 1.220(18), C2-C3 1.370(2), C1-O2 1.228(18), C2-Cl1 1.734(15), C3-N1 1.341(19),

N1-C11 1.469(19), C11-C12 1.487(2) Å and C2-C1-O2 121.74(14), C10-C1-O2 120.19(14), C1-C2-Cl1 114.14(11), C3-C2-Cl1 122.46(12), C5-C4-O1 121.75(13), C3-C4-O1 118.81(13), C3-N1-C11 130.63(13), N1-C11-C12 113.46(12), C2-C3-N1 130.82(14), C4-C3-N1 111.01(12)°, respectively and the structural parameters are found consistent with similar type of compounds reported in the literature (*vide supra*). The amino, methylene and furfuryl groups of **3** behave as X-H donor whereas quinone group is essentially performs are X-H acceptor. For instance, The C14-H14 and C15-H15 groups associated with furfuryl and O2 and Cl11 groups of naphthoquinone are involved in formation of closing contacts with two different molecules *via* C14-H14...O2 and C15-H15...Cl11 donor-acceptor contacts, respectively and these interactions evidently lead to an attractive spiral-like arrangements along *a*-axis as shown in Fig. 4 (b) and (c). It may be noted that C15-H15 group is also involved in the interaction with ketonic O2 group of naphthoquinone. Unlike 1 and 2, the ketonic O2 group in 3 is involved in tri-furcated hydrogen bonding, holding two molecules along *a*-axis through C14-H14$_{(furfuryl)}$...O2 and C15-H15$_{(furfuryl)}$...O2 contacts apart from a molecule *c*-axis through along C11-H11a$_{(methylene)}$...O2. This tri-furcated C-H…O hydrogen bonding interaction arranged the molecules in ac plane an attractive combed shape assembly as shown in Fig. 4(d). Second ketonic group O1 of the molecule present in asymmetric unit forms N1-H1...O1 donor-acceptor closing contact with another molecule and arranging it in '*anti*' fashion in *bc* plane. The relevant parameters for weak interactions present in compound **3** are tabulated in Table 2. The supramolecular unit consists of eight molecules aggregate as shown in Fig. 4(b) which on multiplication, leads to a fascinating 3D supramolecular architecture (Fig. 4(f).

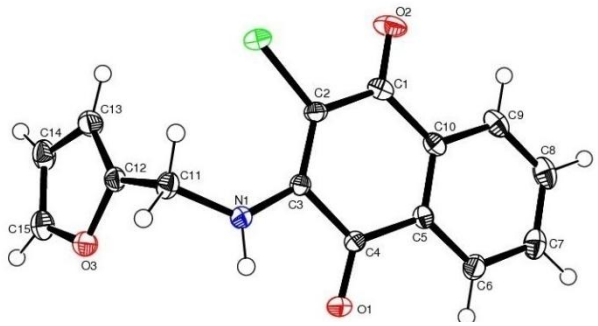

(a)

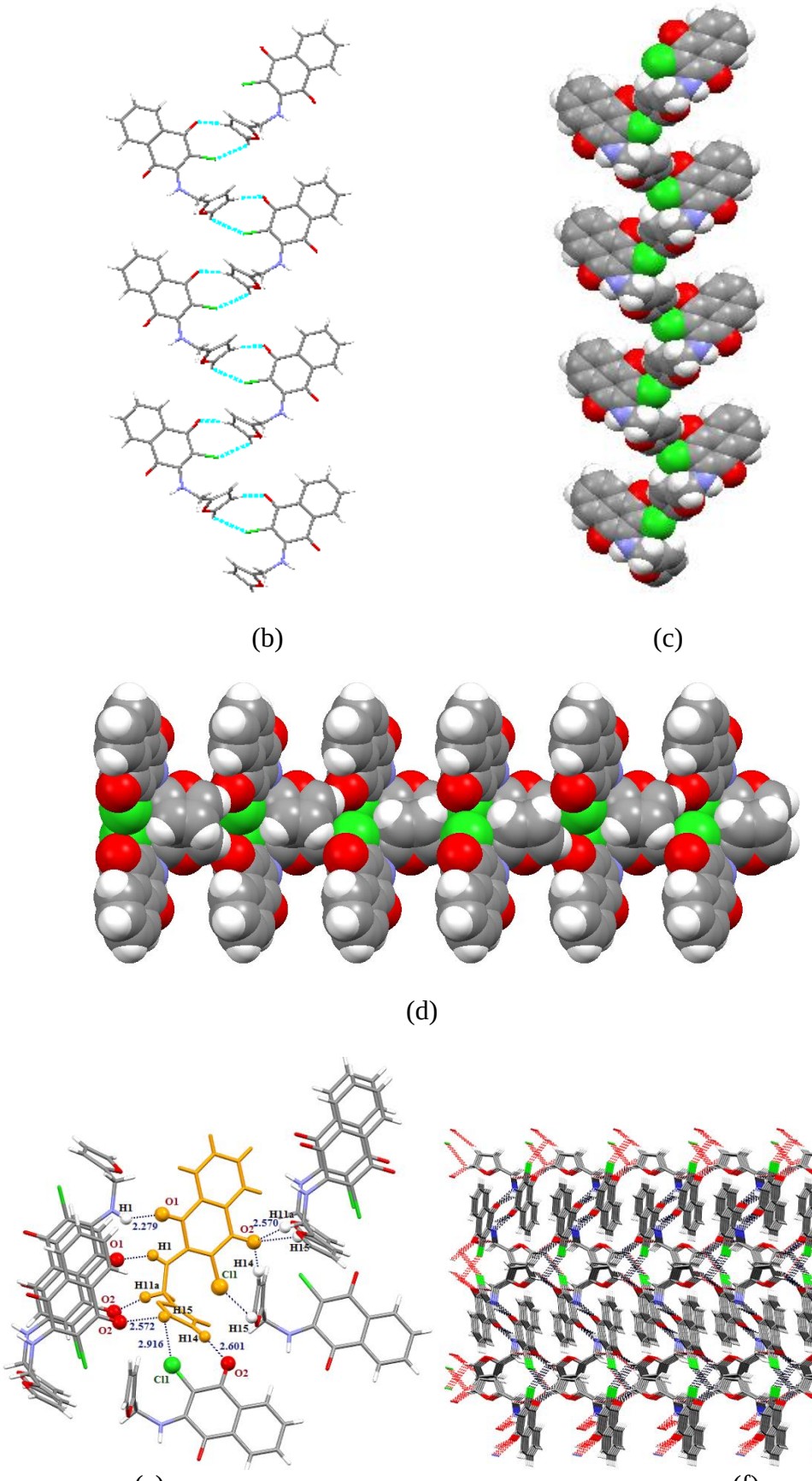

(b) (c)

(d)

(e) (f)

Fig. 4 (a) Thermal ellipsoidal plot of **3** with atom labelling scheme; (b) Formation of spiral shaped molecular arrangement of **3** through C15-H15…Cl and C14-H14…O2

donor-acceptor contacts along *a*-axis; (c) Spacefill representation of spiral shaped assembly; (d) Spacefill representation of an attractive combed shape assembly *via* trifurcated C-H…O hydrogen bonding in *ac* plane; (e) Supramolecular unit consists of eight molecule aggregate involving NH...O, CH...O, CH...Cl hydrogen bonding interactions; (f) Formation of 3D infinite supramolecular architecture in capped stick model, view along *c*-axis.

4A.2.2.4. X-ray structure of 2-(2-pyridylmethylamino)-3-chloro-1,4-naphthoquinone [$C_{16}H_{11}ClN_2O_2$] (4)

Similar to the compounds **2** and **3**, compound **4** bearing *N*-(2-pyridylmethyl) substituent also crystallizes in the centrosymmetric monoclinic P 21/c space group and the X-ray crystal structure show asymmetric unit contains full molecule of [$C_{16}H_{11}ClN_2O_2$] as shown in Fig. 5 (a). There are four such molecules orthogonally arranged in the unit cell. The relevant parameters are tabulated in Table 1. The selected bond distance (Å) and bond angle (°) for **4** are: C9-C10 1.492(5), C9-O1 1.226(4), C15-C16 1.483(5), C16-O2 1.212(4), C9-C8 1.452(5), C16-C7 1.518(5), C8-Cl1 1.736(3), C8-C7 1.371(3), C7-N2 1.338(4), N2-C6 1.449(4), C5-C6 1.513(4) Å and C10-C9-O1 120.4(3), C8-C9-O1 121.6(3), C9-C8-Cl1 114.6(2), C7-C8-Cl1 122.2(3), C15-C16-O2 122.0(3), C7-C16-O2 119.1(3), C7-N1-C6 130.2(3), N2-C7-C16 111.0(3), C5-C6-N2 109.5(3)°, respectively and the structural parameters are found consistent with similar type of compounds reported in the literature (*vide supra*). Of more interesting, the 2-pyridylmethyl substituent on the amino functionality of **4** drastically decreases the dihedral angle and preferentially adopt the lower energy molecular conformation which is nearly coplanar to that of naphthoquinone moiety (dihedral angle 11.12°), offering a large number of sites for weak interactions. The molecules present in the asymmetric unit forms a supramolecular unit consists of six molecules aggregate as shown in Fig. 5(b). For instance, molecules of **4** are arranged in a *zig-zag* fashion, forming a chain along *b*-axis through an emerging C-Cl1... π (Cg1: C10 C11 C12 C13 C14 C15; 3.768 Å) and a cooperative bifurcated hydrogen bonding C4-H4...O1 (2.715 Å), C6-H6B...O1 (2.460 Å) donor-acceptor interactions as shown in Fig 5(c) and Fig 5(d) which is indeed extended along *c*-axis via C2-H2A...O2 (2.593 Å) donor-acceptor contacts. These *zig-zag* chains are apparently translated into orthogonally arranged layers along *c*-axis through cooperative C6-H6A…π (Cg2: C7 C8 C9 C10 C15 C16; 3.472 Å) and C6-H6B….π (Cg3: C1 N1 C2 C3 C4 C5; 3.039 Å) donor-acceptor integrations. The

structural parameters for these interactions are summarized in Table 2. All the three kinds of donor-acceptor interactions provide an opportunity to extend the dimensionality of supramolecular architecture and develop a 3D infinite network (Fig. 5(g)) that illustrates a number of voids along *a*-axis in the spacefill model as shown in Fig. 5(h).

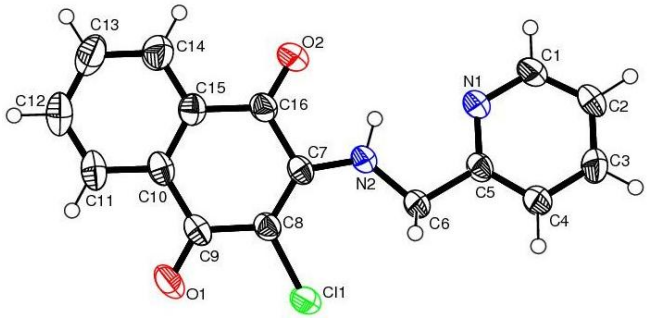

(a)

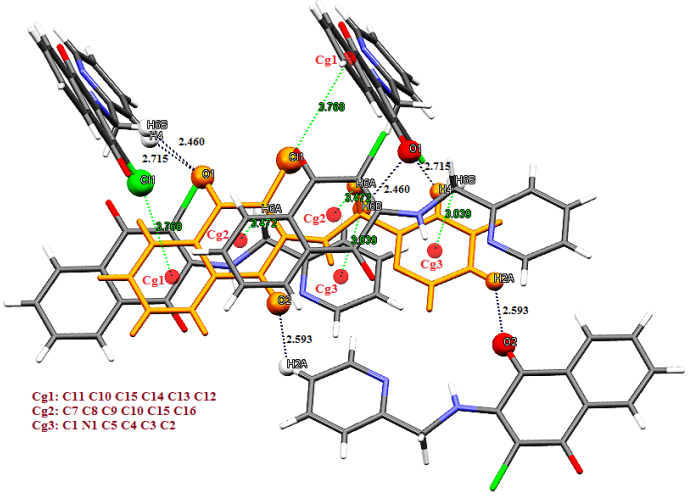

(b)

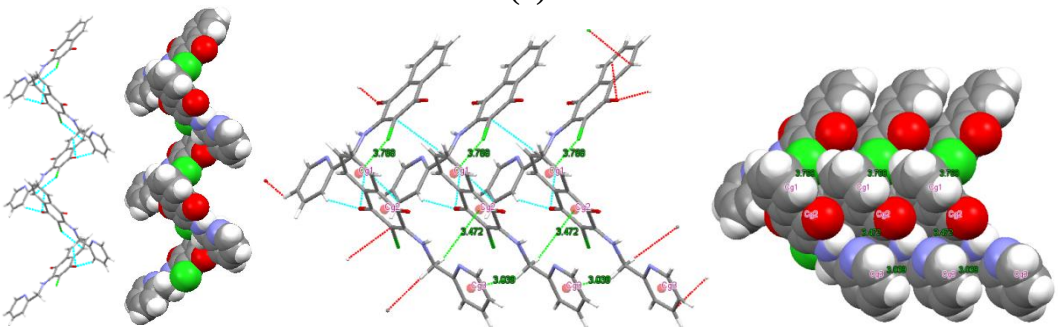

(c) (d) (e) (f)

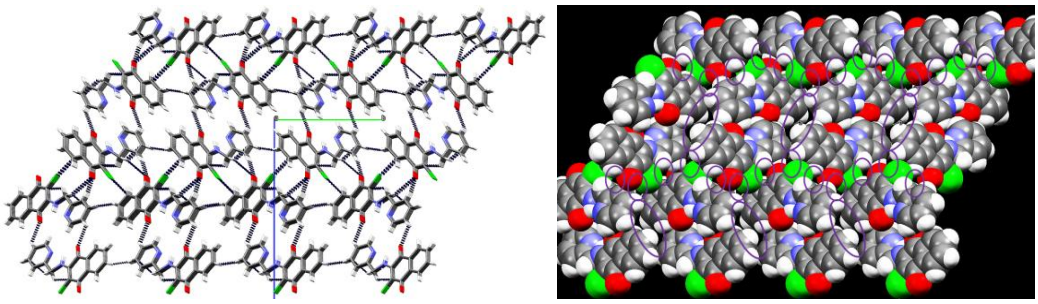

(g) (h)

Fig. 5 (a) Thermal ellipsoidal plot of **4** with atom labelling scheme; (b) Supramolecular unit consists of six molecule aggregate involving CH...O, CH...π and CCl...π interactions; (c) Capped stick and (d) Spacefill representation of orthogonal molecular arrangement of **4** forming *zig-zag* chain along *b*-axis through cooperative C-Cl…Cg1 (C12 C11 C10 C15 C14 C13) and bifurcated C-H…O interactions; (e) Capped stick and (f) Spacefill representation showing translation of zig-zag chains into layers along *c*-axis through cooperative C6H6A…Cg2 (quinone) and C6H6B….Cg3 (pyridine) donor-acceptor integrations; (g) Capped stick and (h) Spacefilled representation of 3D stacking of molecules of **4** along *a*-axis illustrating voids.

4A.2.2.5. X-ray structure of 2-(benzylamino)-1,4-naphthoquinone [$C_{17}H_{13}NO_2$] (7)

Unlike other compounds, compound **7** crystallizes in the polar orthorhombic $Pna2_1$ space group and the X-ray crystal structure show asymmetric unit contains full molecule of [$C_{17}H_{13}NO_2$] as shown in Fig. 6 (a). There are four such molecules arranged parallely along *b*-axis in the unit cell. The relevant parameters are tabulated in Table 1. The selected bond distance (Å) and bond angle (°) for **7** are: C9-C10 1.473(7), C10-O1 1.219(6), C10-C1 1.496(7), C1-C2 1.359(7), C3-C4 1.496(8), C3-O2 1.243(6), C2-C3 1.419(8), C1-N1 1.337(6), N1-C11 1.439(6), C11-C12 1.503(8) Å and C9-C10-O1 122.6(5), C1-C10-O1 119.6(5), C4-C3-O2 119.2(5), C2-C3-O2 121.7(6), C1-N1-C11 124.1(5), N1-C11-C12 116.2(5)°, respectively and the structural parameters are found to be consistent with earlier structure [23b]. Interestingly, presence of the *N*-benzyl substituent and absence of 3-chloro substituent from naphthoquinone, greatly affect the crystal packing pattern of **7**. Surprisingly, it appears that absence of chloro substituent is not affecting the distortion of the naphthoquinone moiety and found almost consistent to that of compound **2**. However, absence of repulsive interaction between chloro group and aromatic substituent leads to nearly orthogonal arrangement of the rings (naphthoquinone and phenyl) possessing dihedral angle of 88.04°. The molecule present in the asymmetric unit exhibit vast number of intermolecular contacts that includes two CH...O, one NH...O,

two CH...π and one π...π donor-acceptor interactions: C2-H2...O1 (2.443 Å), C13-H13...O2 (2.709 Å), N1-H1...O2 (2.168 Å), , and C16-H16...π(Cg1) (3.522 Å), C11-H11b...π(Cg3) (3.480 Å) and π(Cg1)... π(Cg2) (4.187 Å), (where, Cg1: C4 C5 C6 C7 C8 C9; Cg2: C1 C2 C3 C4 C9 C10; Cg3: C12 C13 C14 C15 C16 C17), respectively. Similar to other compounds, one of the ketonic oxygen O2 is involved in bifurcated CH...O interactions. As a result of all these interactions, the molecules present in the asymmetric unit forms a supramolecular unit consists of nine molecules aggregate as shown in Fig. 6(b). The structural parameters for weak interactions observed in compound **7** are tabulated in Table 2. Individually, C2-H2...O1 and C13-H13...O2 donor-acceptor interactions mutually connect the molecules along *a*-axis, while N1-H1...O2 donor-acceptor interactions lead to 1D network in the *ac* plane. Moreover, the π(Cg1)... π(Cg2) and C11-H11B... π(Cg3) interactions mutually involved in the formation of a cavity ~4.187 × 6.922 $Å^2$ and these donor-acceptor interactions contributing for replication of cavities along *c*-axis. Fascinatingly, C16-H16...π(Cg1) donor-acceptor interactions predominantly contribute to 1D stacking of molecules leading to the right handed helical packing along *b*-axis with helical pitch 24.634 Å as shown in Fig. 6(c). When these interactions are extended, it leads to the formation of layers containing helically arranged molecules. Each layer consists of parallel helices (either *P* or *M* helical) separated by ~ 3.769 Å and lower layer consist the opposite helices to that of upper layer. These two layers are forming a grid like structure with cross-section angle of 23.57° and separation distance between layers is ~ 2.901 Å. A view along *a* axis is shown in Fig. 6(d). The mutual effect of all the interactions resulted into a fascinating three dimensional architecture contains a number of openings along *a* axis as shown in Fig. 6(d) and Fig. 6(f).

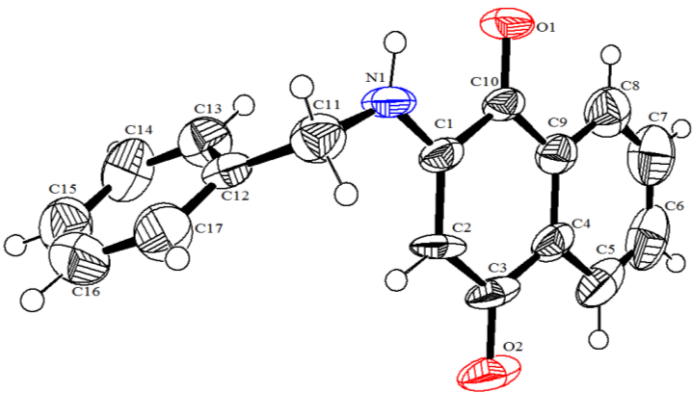

(a)

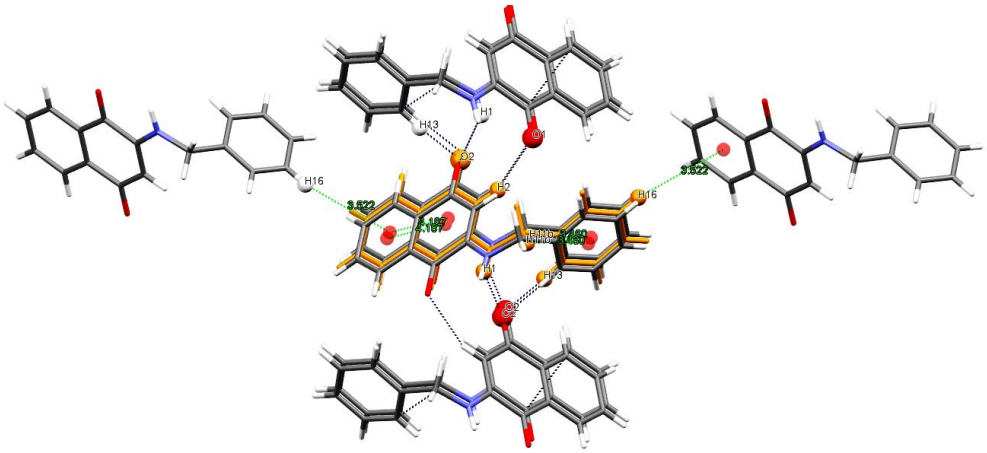
H16
3.822
H1
H43
O1
O2
H2
H16
3.822
H1
H3
O2

(b)

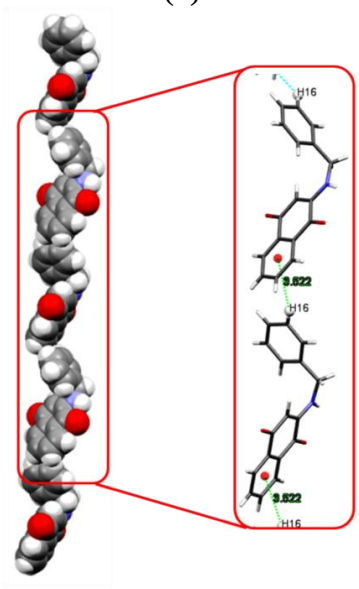
H16
3.822
H16
3.822
H16

(c)

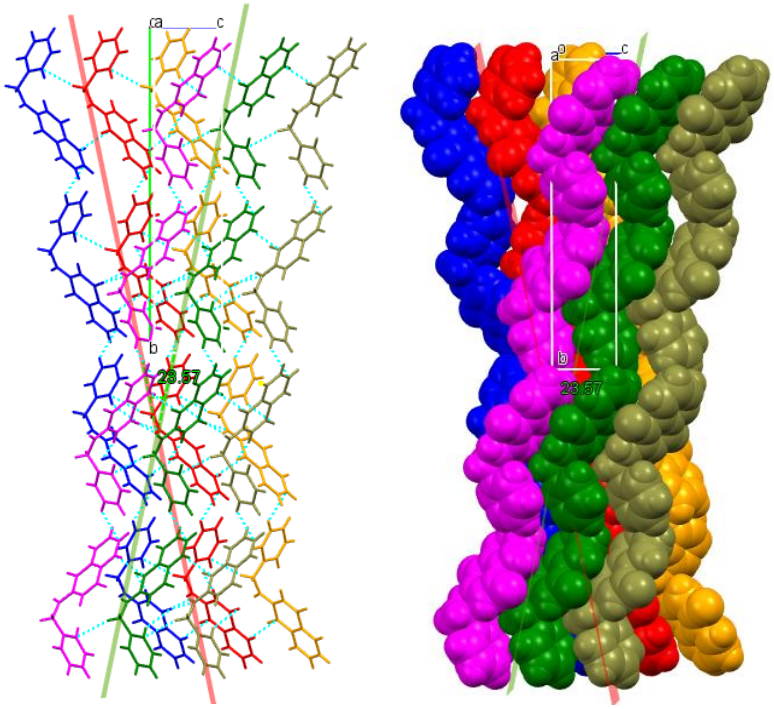
a
c
b
25.57
a
c
b
25.57

(d)

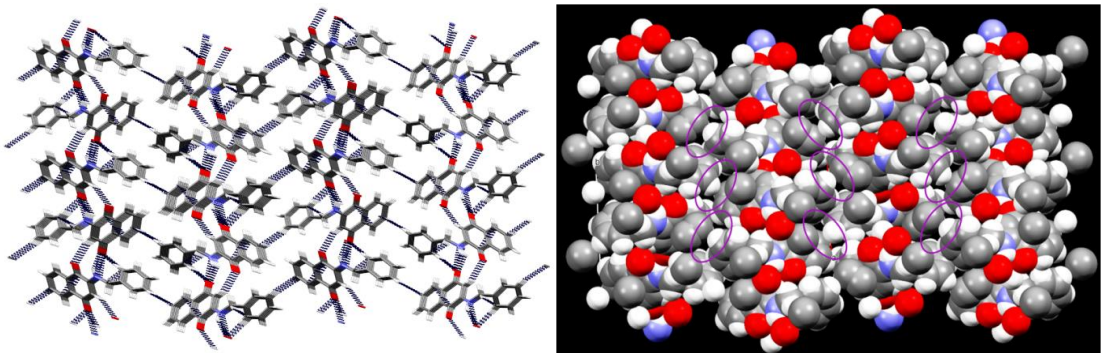

(e) (f)

Fig. 6 (a) Thermal ellipsoidal plot of **7** with atom labelling scheme; (b) Supramolecular unit consists of nine molecule aggregates involving CH...O, CH...π and π...π interactions; (c) Helical packing of **7** along *b* axis through C16-H16...π interactions; (d) Grid like packing of *P* and *M* helical layers in **7**, view along *a* axis; (e) Capped stick view of three dimensional arrangement of molecules along *c* axis; (f) View of molecular packing in spacefilled model along *c*-axis illustrating voids in the packed molecules.

4A.2.3. UV-visible absorption and fluorescence properties

The UV-visible absorption (Fig. 7) and fluorescence spectra (Fig. 8) of all of the compounds **1-7** were obtained at room temperature from 10^{-5} M CH_2Cl_2 solution and 10^{-5} M DMF solution samples respectively and the pertinent results are summarized in Table 3. The assignments of UV-visible absorption and emission bands were performed based upon the absorption and emission spectra of those of closely related compounds [27-29].

The UV-visible absorption spectra of **1-7** showed the expected benzene and naphthoquinone bands in 270–277 nm and 327–334 nm regions mainly arises due to π→π* ectronic transitions [23c]. In addition, a low energy broad band is observed in the visible region centered between 440 nm and 473 nm. This latter absorption is typical of amino-substituted of aminosubstituted benzoquinones, naphthoquinones and anthraquinones [30] and is assigned to CT transitions and weak n→π* transitions of the carbonyl group in the quinone (Table 3). Notably, this broad band in the visible region for compound **1** and **6** showed significant bathochromic shift relative to all other compounds, probably due to +I effects of *N*-cyclohexyl and *N*-n-butyl substituents, respectively.

Table 3 UV-visible absorption and fluorescence spectral data for **1-7**

Entry	UV-visible spectral data (10^{-5} M CH_2Cl_2)			Fluorescence spectral data (10^{-5} M DMF)	
	λ_{max} nm (ε, L Mol^{-1} cm^{-1})	Transitions	Wave number (cm^{-1})	λ_{ex} (nm)	λ_{em} (nm) (Intensity)
1	277 (100205)	π→π*	36036	277	358(5), 613(16)
	334 (8014)	π→π*	29940		
	473 (12985)	n→π*	21142		
2	275 (68146)	π →π*	36364	275	406(43)
	331 (6685)	π→π*	30211		
	461 (8873)	n→π*	21678		
3	273 (102221)	π→π*	36630	--	Not fluorescent
	334 (10534)	π→π*	29940		
	457 (12476)	n→π*	21881		
4	277 (77518)	π →π*	36140	277	418(32), 553(29), 605(36)
	327 (15019)	π→π*	30581		
	465 (8304)	n→π*	21551		
5	273 (90855)	π →π*	36523	273	412(64), 546(21)
	327 (14341)	π→π*	30581		
	459 (10808)	n→π*	21786		
6	276 (80642)	n→π*	36231	--	Not fluorescent
	332 (4558)	π→π*	30120		
	470 (8474)	n→π*	21276		
7	270 (76100)	π →π*	37037	--	Not fluorescent
	330 (8191)	π→π*	30303		
	440 (10312)	n→π*	22727		

Apart from this, fluorescence spectra indicate that the compounds 1,2,4 and 5 fluoresces in the range of 350-620 nm upon excitation at their respective λ_{max} values of 277, 275, 277 and 273 nm, with concomitant Stoke shifts of 81, 131, 141 and 131 nm, respectively. The spectrum of each compound is indeed composed of two broad bands and comparable to those of the closely related compounds [31]. Compound **1** bearing cyclohexyl substituents exhibits weak emission property (5 a.u. at 358 nm and 16 a.u. at 613 nm) from locally excited (π*→π) state at room temperature. However, the alteration of cyclohexyl substituents to benzyl substituents in compound **2** causes significantly increases in fluorescence (43 a.u. at 406 nm). Surprisingly, the fluorescence property of compound **4** (32 a.u. at 418 nm; 29 a.u. at 553 nm) and **5** (64 a.u. at 412 nm; 21 a.u. at 546 nm) differ significantly and infer a great role of the position of pyridyl nitrogen on their fluorescence property. The earlier studies [32, 33] reveal that the fluorescence behavior of molecule is greatly depends upon the arrangement of molecular fragments leading to polymorphism, conformational

rigidity of the fluorophore (dihedral angles), intermolecular interactions π…π or C-H…π interactions and upon the nature of substituents.

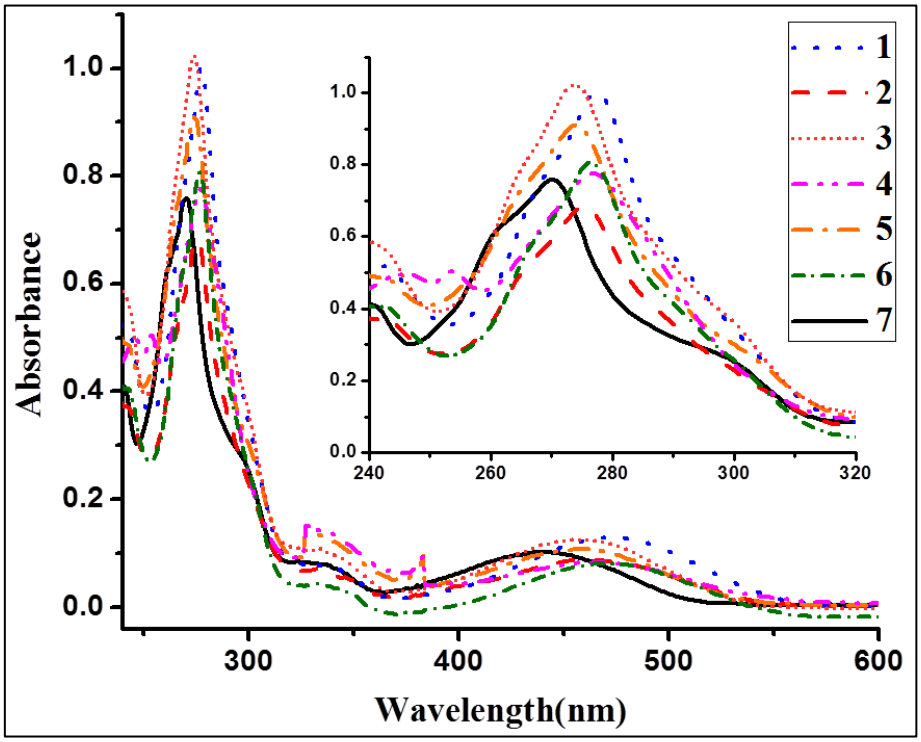

Fig. 7 UV-visible absorption spectra of compounds **1-7** in 10^{-5} M CH_2Cl_2 solution.

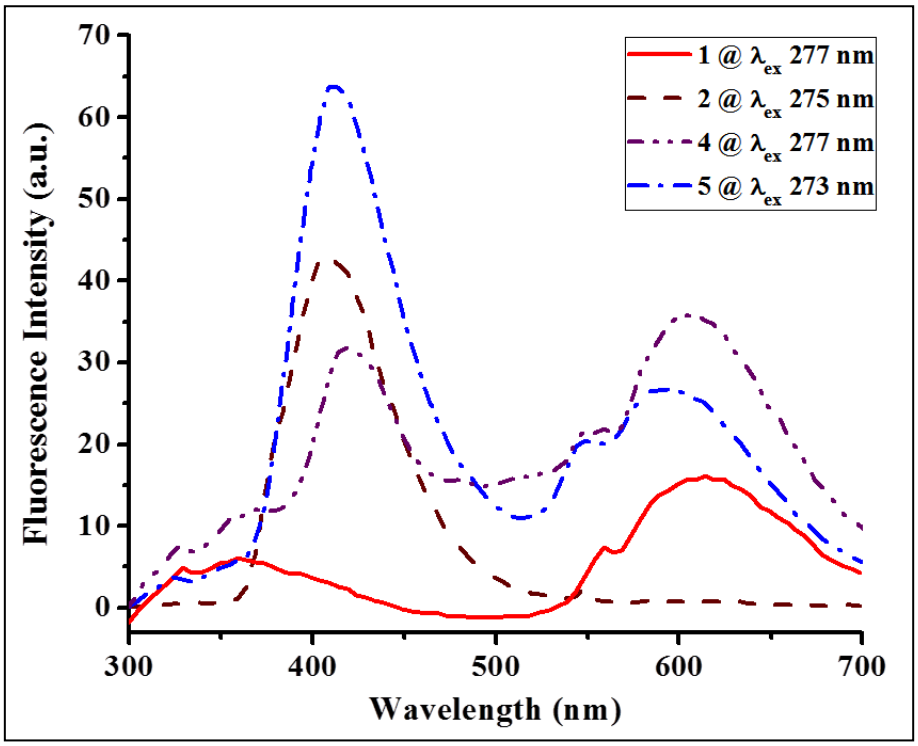

Fig. 8 Fluorescence spectra of compounds **1, 2, 4** and **5** in 10^{-5} M DMF solution.

4A.2.4. Thermogravimetric studies for 1-7

A thermogravimetric study of **1-7**, performed under N_2 atmosphere from room temperature to 750 °C at a heating rate of 10 °C/min, and thermal analysis data of all the compounds is given in Table 4.

Table 4 Thermogravimetric data for **1-7**.

Entry	Mp °C	Mass Loss% (Temperature range °C)	Residual Content	DTG (°C)	DTA (°C)
1	116.7	64 % (200-550)	36 % char	250.6	116.7(endo), 253.3(exo)
2	112.4	62.7 % (180-700)	37.3 % char	201.6, 460	112.4(endo), 201.9(exo)
3	147.3	44.7% (150-700),	Mass loss continues after 750 °C.	173.7, 220.1	147.3(endo), 177.4(exo)
4	160.4	42% (150-700),	Mass loss continues after 750 °C.	161.4	160.4(endo), 192.7(exo)
5	151.8	35.1% (150-700),	Mass loss continues after 750 °C.	146.3	151.8(endo)
6	109.8	64.5% (200-500)	35.5 % char	110.2, 126.9	109.8(endo), 220.6(exo)
7	153.9	92.4% (205-400)	7.6 % char	275.4	153.9 (endo)

A single (compound **1**, **5-7**) or multi (compound **2-4**) stage thermal degradation patterns were observed on TG curves. All the compounds (except 5) exhibit first endothermic peak on the DTA curves without any significant mass loss on corresponding TG curves due to the phase change attributable to the melting points of respective compounds. However, other DTA peaks are attributed to exothermic elimination of molecular fragments due to the thermal degradation, confirmed by DTG curves. Compounds **3-5**, bearing aromatic heterocyclic *N*-substituents appeared to be thermally unstable and the mass loss for these starts at ~150 °C, however other compounds are thermally stable up to 200 °C (supplimentary information Figure S23). Despite of the similar type of molecular framework, the diversity in the thermal stability of these compounds could be attributed to the presence of various intermolecular interactions in the solid state, leading to diverse crystal packing patterns (*vide supra*).

4A.2.5. Cyclic Voltammetric Study

Electrochemical investigations of **1-7** were performed in the potential ranges +0.5 to -2.0 V at scan rate of 50 $mVs^{-1}$from 1.0 mM CH_2Cl_2 solutions containing ^{n}-Bu_4NPF_6

(0.1 M) as supporting electrolyte. The voltammograms for 1-7 are shown in Fig. 9 and electrochemical data is represented in Tables 5. The electrochemical examination of **1-7** clearly demonstrates the quasi-reversible redox behavior of **1**, **2**, **4** and **5.** Similar to the electrochemical behavior of methyl-halogenated naphthoquinones, [34] these compounds primarily exhibit two single-electronic waves due to eletcroredution of naphthoquinone functionality to semiquinone radical anion and then to dianion, respectively. Both the waves are reversible in nature. The separation between each cathodic and corresponding anodic peak, ΔEp at 50 mV/s scan rate is larger than 59 mV (Table 5) and the ratio of the current intensity of the cathodic and anodic peaks are different from unity, suggesting a quasi-reversible nature of both the redox couples of **1**, 2, **4** and **5**. Notably, compound **4** bearing *N*-(2-methylpyridine) substituent displays an additional peak in cathodic scan ($Ep^{\#}c$) as well as in corresponding anodic scan ($Ep^{\#}a$) which resulted into a significant cathodic shift of the electroreduction peaks associated with naphthoquinone moieties, probably due to increased electron density caused by initial electroreduction of 2-pyridine center [35]. However, the voltammograms of other compounds display similar features, except the differences in the cathodic/anodic current peak heights (Fig. 9). Unlike these compounds, the cyclic voltammograms of compounds **3, 6** and **7** display only one single-electronic wave in a cathodic scan due to eletcroredution of naphthoquinone functionality to semiquinone radical anion under similar condition as shown in Fig. 9.

Table 5 Electrochemical data for the compounds **1-7**

Entry	Ep_{Ic}(V)	Ep_{IIc}(V)	$Ep^{\#}{}_{c}$(V)	Ep_{Ia}(V)	Ep_{IIa}(V)	$Ep^{\#}{}_{a}$(V)	ΔEp_{I}(V)	ΔEp_{II}(V)	$\Delta Ep^{\#}$(V)
1	-0.962	-1.555	-	-0.698	-1.151		0.264	0.404	-
2	-0.941	-1.526	-	-0.620	-1.089		0.321	0.437	-
3	-1.145	-	-	-0.537	-1.112		0.608	-	-
4	-1.118	-1.746	-0.480	-0.619	-1.167	-0.274	0.499	0.579	0.206
5	-0.998	-1.606	-	-0.585	-1.108		0.413	0.498	-
6	-1.373	-	-	-0.619	-1.284		0.754	-	-
7	-1.348	-	-	-0.785	-1.343		0.563	-	-

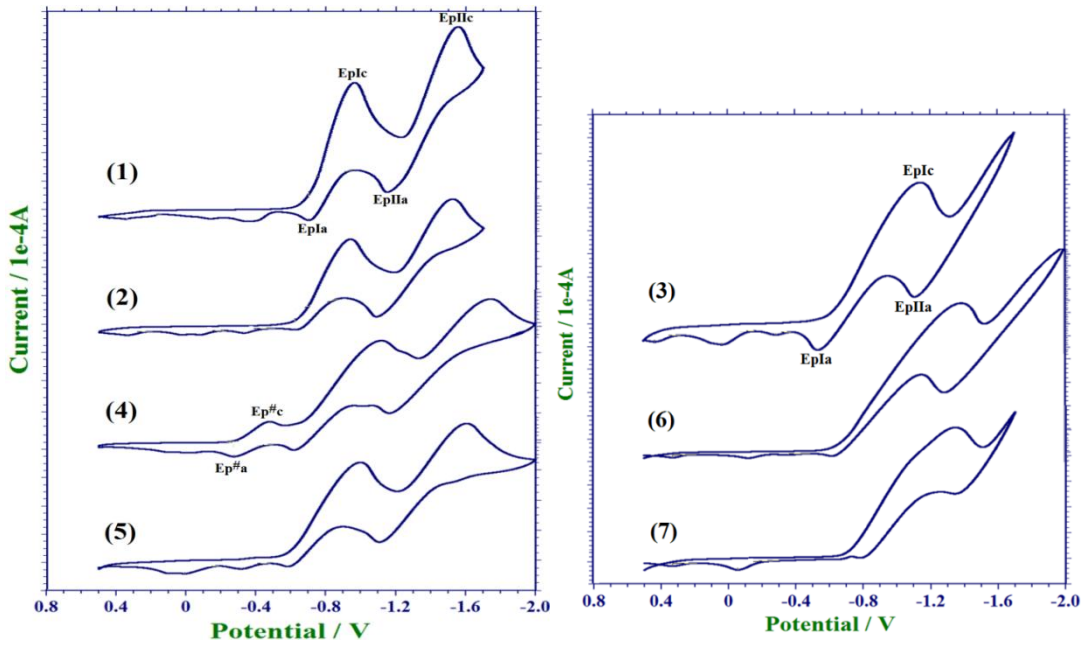

Fig. 9 Cyclic voltammograms of a 1 mM solution of compounds **1-7** in CH_2Cl_2 containing 0.1 M tetra-n-butylammonium hexafluorophosphate as the supporting electrolyte.

4A.2.6. Biological evaluation

In the light of antibacterial action of quinines [36] all the naphthoquinone derivatives 1-7 were screened for their antibacterial activity against two gram positive bacteria S. aureus and B. subtilis and two gram negative bacteria E. coli and P. aeruginosa by Broth dilution method [37]. These compounds were further evaluated for their in vitro antifungal activity against C. albicans and A. niger. Concentration of compounds was varied from 10 µg/ml to 600 µg/ml. Analysis suggests that solvent had no antibacterial or antifungal activities against any of the tested microorganisms. For comparison purpose, two standard drugs ciprofloxacin and flucanazole were taken as reference and tested under the similar conditions. The lowest concentrations of the compounds that prevented visible growth *i. e.* minimum inhibitory concentration (MIC) of the naphthoquinone derivatives **1-7** against inhibited organisms is summarized in Table 6. A careful comparison of antibacterial activity of compounds 1–7 with a well known antibaterial drug ciprofloxacin (MIC against S. Aureus: 15 µg/ml and MIC against B. Subtilis: 5 µg/ml) showed that compounds **4** and 5 showed best activity against both of the gram positive bacteria S. aureus and B. Subtilis (Table 6). However, compounds **1, 3, 6** and **7** displays less activity against both of the gram

positive bacteria, except compound **6** performing moderate activity against B. Subtilis. Further results suggest that all compounds exhibit moderate activity against both of the gram negative bacteria, except compound **2** performing less activity against E. coli. The presence of N-methylpyridine substituents in **4** and **5** is apparently brings them about extreme potent activity against both of the gram positive bacteria. Remarkably, compound **5** exhibits enhanced antibacterial activity against S. Aureus and proved to be more potent antibacterial agent than ciprofloxacin. All these naphthoquinone derivatives showed high MIC values (600 µg/ml) against both of the fungus, except compounds **4** and **5** bearing pyridine N-substituents, performing moderate (MIC 300 µg/ml) activity against C. Albicans (Fig. 10).

Table 6 MIC determination of antibacterial and antifungal agent (µg/ml)

Entry	MIC (µg/ml)					
	S. aureus	B. subtilis	E. coli	P. aeruginosa	C. albicans	A. niger
	(gm +ve bacteria)		(gm -ve bacteria)		(Fungi)	
1	>600	600	200	200	>600	>600
2	200	100	600	200	>600	>600
3	>600	600	300	200	>600	>600
4	20	10	300	300	300	>600
5	10	10	200	200	300	>600
6	600	300	300	200	600	>600
7	>600	>600	200	200	>600	>600
Ciprofloxacin	15	5	15	10	-	-
Flucanazole	-	-	-	-	10	40

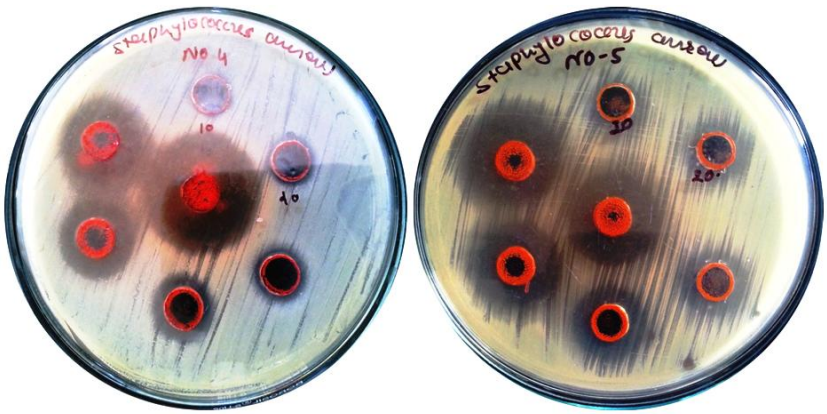

Fig. 10 Zone of inhibition of compound 4 and 5 of antibacterial against Staphylococus aureus

In general, the naphthoquinone derivatives are found to exhibit better anti-microbial properties than a number of recently reported coumarin derivatives [38] against the

same set of microbes. Further comparison of antibacterial properties of **4** and **5** with those of closely related compounds [16e,39] against S. aureus, suggest that these compounds showed better activity than a number of 1,4-naphthoquinone derivative such as 2-Arylamino-3-chloro-1,4-naphthoquinones, 2-Amino-3-arylsulfanyl-1,4-naphthoquinones, 2-Arylamino-3-arylsulfanyl-1,4-naphthoquinones.

4A.3. Conclusion

This study allows us to conclude that the introduction of various amine *N*-substituents in **1-4** and **7** induces conformational changes that apparently modify the nature and number of donor-acceptor sites for noncovalent interactions, leading to diverse crystal packing patterns. The *N*-(phenylmethyl)- and *N*-(2-pyridylmethyl)- substituents in **2** and **4**; successfully lead to the opening of an emerging C-H...π synthon, scarcely seen in the crystal packing of organic molecules. This synthon, efficiently managed the *anti* orientation of molecules of **2** and limits the growth of self-assembly along *c*-axis, however, the self-assembly can be extended along *b*-axis through cooperative C-H...O and N-H...O interactions leading to the fascinating 1D infinite supramolecular chair-like architecture. The molecules of **4** are arranged in a *zig-zag* fashion, forming a chain along *b*-axis *via* cooperative C-Cl... π and bifurcated hydrogen bonding. The mutual effect of all interactions in **4** resulted into the formation of fascinating 3D infinite network, illustrating a number of openings along *a*-axis in the spacefill model. The fluorescence study indicates that the compounds **1, 2, 4** and **5** fluoresces in the range of 350-620 nm with concomitant Stoke shifts of 81, 131, 141 and 131 nm, respectively and their cyclic voltammograms evidence two quasi-reversible single-electron waves. All the compounds (except 5) exhibit first endothermic peak on the DTA curves without any significant mass loss on corresponding TG curves due to the phase change attributable to the melting points of respective compounds. A careful comparison of antibacterial activity of compounds 1–7 with a well known antibaterial drug ciprofloxacin (MIC against S. Aureus: 15 µg/ml and MIC against B. Subtilis: 5 µg/ml) showed that **4** and 5 showed best activity against both of the gram positive bacteria S. aureus and B. Subtilis. The presence of *N*-pyridylmethyl substituents in **4** and **5** is apparently brings them about extreme potent activity against S. aureus and B. Subtilis. Interestingly, compound **5** exhibits enhanced antibacterial activity against S. Aureus and proved to be more potent antibacterial agent than ciprofloxacin.

4A.4. Experimental Section

4A.4.1. Material and physical measurements

All the chemicals and solvents used in this work were of laboratory grade available at various commercial sources and used without further purification. Melting points were recorded in open capillaries and uncorrected. Thin Layer Chromatography was performed on Merck 60 F254 aluminium coated plates. Elemental analyses (C, H, N) were performed on a Perkin-Elmer 2400 analyzer. Mass spectra were obtained on Thermo-Fischer DSQ II GCMS instrument. FT-IR (KBr pellets) spectra were recorded in the 4000-400 cm^{-1} range using Perkin-Elmer FT-IR spectrometer. The NMR spectra were obtained on a Bruker AV-III 400 MHz spectrometer in $CDCl_3$ solvent. UV-visible spectra were recorded on a Perkin Elmer Lambda 35 UV-visible spectrophotometer and the optical characterization of solid samples was performed by using the UV-visible transmittance measurements. Fluorescence was recorded on JASCO make spectrofluorometer model FP-6300. TGA/DTA plots were obtained using SII TG/DTA 6300 in flowing N_2 with a heating rate of 10 °C min^{-1}. Electrochemical measurements were performed on a CH Instruments 600C potentiostat, using a Pt disk as the working electrode, Ag/AgCl as the reference electrode and a Pt wire as the counter electrode. Voltammograms were recorded by using anhydrous solutions of the amines (put general name) in CH_2Cl_2 solutions (1.0mM) containing tetra-n-butylammonium hexafluorophosphate (0.1M) as supporting electrolyte. The synthesized compounds were screened for their in vitro antibacterial activity against S. Aureus, B. Subtilis, E. Coli, P. aeruginosa and antifungal activity against C. albicans, A. niger at the Division of Centralnkashiba Advance Diagnostic Laboratory, Surat, Gujarat, India.

4A.4.2. Synthesis of compounds 1-7

4A.4.2.1. General procedure for synthesis of 2-(alkylamino)-3-chloro-1,4-naphthoquinones (1-6)

To yield a series of 2-(alkylamino)-3-chloro-1,4-naphthoquinone derivatives, corresponding amine (cyclohexyl amine (0.5 mL, 4.404 mmol), benzyl amine (0.481 mL, 4.404 mmol), furfuryl amine (0.427 mL, 4.404 mmol), 2-picolyl amine (0.476 mL, 4.404 mmol), 3-picolyl amine (0.475 mL, 4.404 mmol) or n-butyl amine (0.460 mL, 4.404 mmol) was added in 30 mL of absolute ethanol containing 1 equivalent of

2,3-dichloro-1,4-napthaquinone (1g, 4.404 mmols). The reaction mixture was stirred at room temperature for 6 hours. During these hours, a change in the colour of the reaction mixture was observed from yellow to red. The progress of the reaction was monitored by the TLCs. The reaction mixture was dried under vacuum and the residue was washed several times with saturated Na_2CO_3 solution followed by 3 × 10 mL of distilled water. The red coloured product was finally dried under vacuum and preserved in desiccator for analysis. The elemental analysis, FT-IR and NMR data for compounds **1-6** are given as follows:

1. Yield 1260.25 mg, 99%. M.p. 116.7 °C. Elemental analysis: Calcd. for $C_{16}H_{16}ClNO_2$ (289.09): C, 66.32; H, 5.57; N, 4.83. Found: C, 66.80; H, 5.68; N, 4.79. ES-MS: 290.61 (M+H), (50%); 287.76 (M-2H), (100%). IR (KBr disc, cm^{-1}): 3303s, 2931m, 2852m, 1675s, 1634m, 1596s, 1564s, 1515s, 1451m, 1331s, 1291s, 1251m, 1234m, 1154m, 1132m, 1079w, 963w, 847w, 822w, 783w, 722s, 679m, 647w, 619m, 560w, 544w, 467w. ^{1}H NMR (400 MHz, $CDCl_3$): δ (ppm) 8.17 (dd, 1H, -Ph), 8.06 (dd, 1H, -Ph), 7.75 (td, 1H, -Ph), 7.63 (td, 1H, -Ph), 6.12 (s, 1H; NH), 4.44 (m, 1H, CH), 2.09 (dd, 2H, CH_2), 1.80 (m, 2H, CH_2), 1.38 (m, 6H, CH_2). ^{13}C NMR: δ (ppm) 180.6 (C=O), 177 (C=O), 134.9 (C-N), 132.8, 132.4, 129.7, 126.8 (all corresponds to the carbons of Ph), 52.5, 34.6, 25.3, 24.5 (all corresponds to the carbons of cyclohexyl moiety).

2. Yield: 1242.61 mg, 95%. M.p. 112.4 °C. Elemental analysis: Calcd. for $C_{17}H_{12}ClNO_2$ (297.06): C, 68.58; H, 4.06; N, 4.70. Found: C, 68.35; H, 4.22; N, 4.65. ES-MS: 297.78 (M+H); (40%). IR (KBr disc, cm^{-1}): 3279s, 2935w, 1683s, 1638m, 1598s, 1565s, 1516s, 1443m, 1332s, 1299s, 1254s, 1136m, 1066m, 1029m, 934w, 913w, 867w, 823m, 753m, 725s, 699s, 680m, 607m, 595m, 545m, 494m, 445m. ^{1}H NMR (400 MHz, $CDCl_3$): δ (ppm) 8.18 (dd, 1H, -Ph), 8.058 (dd, 1H, -Ph), 7.75 (td, 1H, -Ph), 7.65 (td, 1H, -Ph), 6.26 (s, 1H, NH), 7.3 (m, 5H, -Ph), 5.07(s, 2H, CH_2). ^{13}C NMR: δ (ppm) 180.4 (C=O), 176.9 (C=O), 144 (C-N), 137.8, 134.9, 132.6, 129.7, 129, 128, 127.7, 126.9 (all corresponds to the carbons of Ph), 48.9 (benzylic CH_2).

3. Yield: 1175.32 mg 93%. M.p. 147.3 °C. Elemental analysis: Calcd. for $C_{15}H_{10}ClNO_3$ (287.03): C, 62.62; H, 3.50; N, 4.87. Found: C, 62.55; H, 3.49; N, 4.95. ES-MS: 286.27 (M-H), (100%); 287.20 (M), (56%); 288.19 (M+H), (37%). IR (KBr disc, cm^{-1}): 3324s, 3147w, 3125w, 1680s, 1639m, 1599s, 1569s, 1519s,

1431m, 1357m, 1334m, 1300s, 1250s, 1205m, 1139s, 1064s, 1008m, 933m, 901w, 864w, 823w, 756s, 721s, 693m, 679m, 605m, 550m, 478m. ^{1}H NMR (400 MHz, $CDCl_3$): δ (ppm) 8.16 (dd, 1H, -Ph), 8.05 (dd, 1H, -Ph), 7.75 (td, 1H, -Ph), 7.65 (td, 1H, -Ph), 6.23 (s, 1H; NH), 7.42 (d, 1H, CH of furanyl moiety), 6.35-6.38 (m, 2H, CH of furanyl moiety), 5.08(s, 2H, CH_2). ^{13}C NMR: δ (ppm) 180.3(C=O), 176.9(C=O), 150.6 (C-N), 143.8, 142.8, 134.9, 132.6, 132.5, 129.8, 126.9, 110.6, 108.4 (all corresponds to the carbons of Ph/furanyl moiety), 41.8 (benzylic CH_2).

4. Yield: 1194.17 mg 91%. M.p. 160.4 °C. Elemental analysis: Calcd. for $C_{16}H_{11}ClN_2O_2$ (298.05): C, 64.33; H, 3.71; N, 9.38. Found: C, 64.55; H, 3.79; N, 9.35. ES-MS: 298.55 (M+H), (5%), 262.79 (100%). IR (KBr disc, cm^{-1}): 3252s, 3067w, 1683s, 1605s, 1575s, 1566s, 1496s, 1480m, 1444m, 1432m, 1330s, 1295s, 1288s, 1251m, 1208m, 1139m, 1016m, 839m, 760m, 719s, 679m, 639w, 547m. ^{1}H NMR (400 MHz, $CDCl_3$): δ (ppm) 8.68 (d, 1H, -Py), 8.19 (dd, 1H, -Ph), 8.10 (dd 1H, -Ph), 7.75 (td, 1H, -Ph), 7.67 (td, 1H, -Ph), 7.34 (m, 3H, Py), 7.82 (s, 1H, NH), 5.22 (s, 2H, CH_2). ^{13}C NMR: δ (ppm) 180.6 (C=O), 176.8 (C=O), 155.1, 148.7, 144.3, 137.3, 134.8, 132.6, 132.5, 129.9, 126.8, 126.7, 122.8, 121.9 (all corresponds to the carbons of Ph/pyridyl moiety), 48.4 (benzylic CH_2).

5. Yield: 1181.28 mg 90%. M.p. 151.8 °C. Elemental analysis: Calcd. for $C_{16}H_{11}ClN_2O_2$ (298.05): C, 64.33; H, 3.71; N, 9.38. Found: C, 64.37; H, 3.68; N, 9.31. ES-MS: 297.65 (M-H), (5%). IR (KBr disc, cm^{-1}): 3171m, 3007w, 1683s, 1644m, 1601s, 1572s, 1521s, 1444m, 1424m, 1328s, 1292s, 1255s, 1184w, 1136s, 1063m, 1035w, 1028w, 820w, 795w, 723m, 708m, 680w, 635w, 612m, 547m, 503w, 451w. ^{1}H NMR (400 MHz, $CDCl_3$): δ (ppm) 8.66 (d, 1H, -Py), 8.61 (dd, 1H, -Py), 8.18 (dd 1H, -Ph), 8.07 (dd, 1H, -Ph), 7.75 (td, 1H, -Ph), 7.67 (td, 1H, -Ph), 7.40 (m, 1H, -Py), 7.75 (m, 1H, -Py), 6.31 (s, 1H, NH), 5.11 (s, 2H, CH_2). ^{13}C NMR: δ (ppm) 180.3(C=O), 176.9(C=O), 149.4, 149.0, 143.7, 135.2, 135, 135, 133.7, 132.7, 129.7, 126.9, 123.8 (all corresponds to the carbons of Ph/pyridyl moiety), 46.2 (benzylic CH_2).

6. Yield: 1077.61 mg 93%. M.p. 109.8 °C. Elemental analysis: Calcd. for $C_{14}H_{14}ClNO_2$ (263.07): C, 63.76; H, 5.35; N, 5.31. Found: C, 63.95; H, 5.29; N, 5.35. ES-MS: 262.04 (M-H), (26%). IR (KBr disc, cm^{-1}): 3279s, 3064m, 1651s, 1559s, 1507w, 1499m, 1456m, 1427s, 1365m, 1237s, 1172w, 1164w, 1063s,

1031m, 1003w, 924w, 785w, 744m, 726s, 698s, 591m, 556s, 505s, 418w. ^{1}H NMR (400 MHz, $CDCl_3$): δ (ppm) 8.18 (dd, 1H, -Ph), 8.059(dd, 1H, -Ph), 7.74 (td, 1H, -Ph), 7.64 (td, 1H, -Ph), 6.10 (s, 1H, NH), 3.88 (t, 2H, CH_2), 1.70 (m, 2H, CH_2), 1.48 (m, 2H, CH_2), 1.43 (t, 3H, CH_3). ^{13}C NMR: δ (ppm) 180.6 (C=O), 176.9 (C=O), 134.9, 132.8, 132.4, 129.7, 126.8 (all corresponds to the carbons of Ph), 44.7, 33, 19.8(all corresponds to CH_2), 13.7 (CH_3).

4A.4.2.2. General procedure for synthesis of 2-(benzylamino)-1,4-naphthoquinone (7)

2,3-dichloro-1,4-napthaquinone (300 mg, 1.321 mmol) and benzyl amine (0.288 mL, 2.642 mmol) were added in 10 mL of DMF and the reaction mixture was allowed to reflux for 4 hours. Reaction progress was monitored by TLC. The reaction mixture was cooled at room temperature. The reaction mixture was then quenched with of ice cold water and the crude product was recovered by vacuum filtration. The desired compound was purified by column chromatography (1:5 ethyl acetate: petroleum ether) to yield a red coloured solid.

7. Yield: 271.24 mg, 78%. m.p. 162 °C. Elemental analysis: Calcd. for $C_{17}H_{13}NO_2$ (263.09): C, 77.55; H, 4.98; N, 5.32. Found: C, 77.67; H, 5.05; N, 5.41. ES-MS: 262.85, 263 (M+H); (100%). IR (KBr disc, cm^{-1}): 3333s, 3061w, 1683s, 1594s, 1563s, 1503s, 1452m, 1440m, 1360s, 1338s, 1305m, 1259s, 1216m, 1151w, 1124s, 1097w, 1066m, 1027w, 1006m, 943s, 846s, 782m, 728s, 694m, 609m, 547m, 482m, 458w, 451w, 416m. ^{1}H NMR (400 MHz, $CDCl_3$): δ (ppm) 8.115 (dd, 1H, -Ph), 8.082(dd, 1H, -Ph), 7.755 (td, 1H, -Ph), 7.66 (td, 1H, -Ph), 6.25 (s, 1H, NH), 7.38 (m, 5H, Ph), 5.82 (s, 1H, -Ph), 4.07(s, 2H, CH_2). ^{13}C NMR: δ (ppm) 183.1 (C=O), 181.9 (C=O), 147.7, 135.9, 134.8, 133.5, 132.1, 130.5, 129, 128.2, 127.7, 126.3, 126.2, 101.7 (all corresponds to the carbons of Ph), 46.8(CH_2).

4A.4.3. X-ray crystallography and data collection

Crystals of **1-4** and **7** suitable for X-ray crystallographic study were obtained in dichloromethane by slow evaporation at 4 °C. Intensity data were collected on Oxford diffraction X Calibur diffractometer equipped with Eos CCD detector at 150 K for $[C_{16}H_{16}ClNO_2]$ **1**, $[C_{17}H_{12}ClNO_2]$ **2**, $[C_{15}H_{10}ClNO_3]$ **3,** $[C_{16}H_{11}ClN_2O_2]$ **4** and

$[C_{17}H_{13}NO_2]$ **7**, respectively. Monochromatic Mo-*Kα* X-ray (λ=0.71073 Å) was used for the measurements. Data were collected and reduced by using the ‘‘CrysAlispro’’ program [40]. An empirical absorption correction using spherical harmonics was implemented in ‘‘SCALE3 ABSPACK’’ scaling algorithm. The crystal structures were solved by direct methods using SHELXL-97 [41] and the refinement was carried out against F^2 using SHELXL-97 program package [42]. All non-hydrogen atoms were refined anisotropically. Electronic Supplementary Information (ESI) available: Additional figures and CIF files. See CCDC reference numbers 986339 for **1**; 986337 for **2**; 986340 for **3**; 986336 for **4** and 986338 for **7**.

4A.5. References

1 (a) Hulme, A. T.; Price S. L.; Tocher, D. A. *J. Am. Chem. Soc*. **2005**, *127*, 1116; (b) Kirchner, M. T.; Bläser, D.; Boese, R. *Chem. Eur. J*. **2010**, *16*, 2131.

2 Desiraju, G. R. *Curr. Opin. Solid State Mater. Sci*. **1997**, *2*, 451.

3 (a) Gu, Y.; Kar, T.; Scheiner, S. *J. Am. Chem. Soc*. **1999**, *121*, 9411; (b) Derewenda, Z. S.; Lee L.; Derewenda, U. *J. Mol. Biol*. **1995**, *252*, 248; (c) Desiraju, G. R.; Steiner, T.; The Weak Hydrogen Bond: In Structural Chemistry and Biology, Oxford University Press, New York, 2001; (d) Hobza, P.; Havlas, Z. *Chem. Rev*. **2000**, *100*, 4253; (e) Desiraju, G. R. *Acc. Chem. Res*. **1996**, *29*, 441; (f) Taylor R.; Kennard, O. *J. Am. Chem. Soc*.**1982**, *104*, 5063.

4 (a) Mukherjee, G.; Biradha, K. *J. Chem. Sci*, **2014**, *126*, 1285; (b) Scheiner, S. *Phys. Chem. Chem. Phys*. **2011**, *13*, 13860.

5 (a) Nishio, M. *CrystEngComm*, **2004**, *6*, 130; (b) Nishio, M.; Umezawa, Y.; Honda, K.; Tsuboyama S.; Suezawa, H. *CrystEngComm*, **2009**, *11*, 1757; (c) Takahashi, O.; Kohno, Y.; Nishio, M. *Chem. Rev*. **2010**, *110*, 6049; (d) Nayak, S. K.; Sathishkumar R.; Guru Row, T. N. *CrystEngComm*, **2010**, *12*, 3112; (e) Takahashi, O.; Kohno, Y.; Iwasaki, S.; Saito, K.; Iwaoka, M.; Tomoda, S.; Umezawa, Y.; Tsuboyama S.; Nishio, M. *Bull. Chem. Soc. Jpn*, **2001**, *74*, 2421; (f) Tewari, A. K.; Dubey, R. *Bioorg. Med. Chem*, **2008**, *16*, 126; (g) Kobayashi, Y.; Saigo, K. *J. Am. Chem. Soc*., **2005**,*127*, 15054; (h) Saigo, K.; Kobayashi, Y. *Chem. Rec*. **2007**, *7*, 47; (i) Sozzani, P.; Comotti, A.; Bracco, S.; Simonutti, R. *Chem. Commun*. **2004**, 768; (j) Hill, J. P.; Scipioni, R.; Boero, M.; Wakayama, Y.; Akada, M.; Miyazaki, T.; Ariga, K. *Phys. Chem. Chem. Phys*. **2009**, *11*,

6038; (k) Tiekink E. R. T.; Schpector, J. Z. The Importance of Pi-Interactions in Crystal Engineering: Frontiers in Crystal Engineering, John Wiley & Sons Inc., 2012; (l) Nishio, M. *Phys. Chem. Chem. Phys*. **2011**, *13*, 13873; (m) Nishio, M. *J. Mol. Struct*. **2012**, *1018*, 2.

6 (a) Hunter, C. A.; Sanders, J. K. M. *J. Am. Chem. Soc*. **1990**, *112*, 5525; (b) Hunter, C. A. *Chem. Soc*. *Rev*. **1994**, *23*, 101; (c) Janiak, C. *J. Chem. Soc. Dalton Trans*. **2000**, 3885; (d) Headen, T. F.; Howard, C. A.; Skipper, N. T.; Wilkinson, M. A.; Bowron, D. T.; Soper, A. K. *J. Am. Chem. Soc.* **2010**, *132*, 5735; (e) Kadu, R.; Singh, V. K.; Verma, S. K.; Raghavaiah P.; Shaikh, M. M. *J. Mol. Struct.* **2013**, *1033*, 298.

7 (a) Metrangolo, P.; Neukirch, H.; Pilati. T.; Resnati, G. *Acc. Chem. Res*. **2005**, *38*, 386; (b) Rissanen, K. *CrystEngComm*, **2008**, *10*, 1107; (c) Metrangolo, P.; Meyer, F.; Pilati, T.; Resnati, G.; Terraneo, G. *Angew. Chem., Int. Ed*. **2008**, *47*, 6114.; (d) Metrangolo, P.; Carcenac, Y.; Lahtinen, M.; Pilati, T.; Rissanen, K.; Vij, A.; Resnati, G. *Science*, **2009**, *323*, 1461; (e) Bertani, R.; Sgarbossa, P.; Venzo, A.; Lelj, F.; Amati, M.; Resnati, G.; Pilati, T.; Metrangolo, P.; Terraneo, G. *Coord. Chem. Rev*. **2010**, *254*, 677.

8 (a) Swierczynski, D.; Luboradzki, R.; Dolgonos, G.; Lipkowski, J.; Schneider, H. –J. *Eur. J. Org. Chem*. **2005**, 1172 (b) Brammer, L.; Espallagras, G. M.; Libri, S. *CrystEngComm*, **2008**, *10*, 1712.

9 (a) Auffinger, P.; Hays, F.; Westhof, E.; Ho, P. S. *Proc. Natl. Acad. Sci*. U. S. A. **2004**, *101*, 16789; (b) Voth, A. R.; Hays, F. A.; Ho, P. S.*Proc. Natl. Acad. Sci*. U. S. A. **2007**, *104*, 6188.

10 (a) Glaser, R.; Chen, N.; Wu, H.; Knotts, N.; Kaupp, M. *J. Am. Chem. Soc*. **2004**, *126*, 4412; (b) Shishkin, O. V.; Khrustalev, V. N.; Lindeman, S. V.; Yu. Ukhin, Zh, L.; Orlova I. T. N. *Kristallogr*. **1998**, *213*, 296.

11 (a) Legon, A. C. *Chem. Phys. Lett*. **1999**, *314*, 472; (b) Legon, A. C. *Angew. Chem., Int. Ed*., **1999**, *38*, 2686.

12 (a) Aakeroy, C. B.; Fasulo, M.; Schultheiss, N.; Desper, J.; Moore, C. *J. Am. Chem. Soc*. **2007**, *129*, 13772; (b) Bouchmella, K.; Boury, B.; Dutremez, S. G.; van der Lee, A. *Chem. Eur. J*. **2007**, *13*, 6130.

13 Espallargas, G. M.; Zordan, F.; Marin, L. A.; Adams, H.; Shankland, K.; van der Streek, J.; Brammer, L. *Chem. Eur. J*. **2009**, *15*, 7554.

14 (a) Nie, Y.; Miao, J.; Pritzkow, H.; Wadepohl, H.; Siebert, W. *J. Organomet. Chem*. **2013**, *747*, 174; (b) Hathwar, V. R.; Roopan, S. M.; Subashini, R.; Khan, F. N.; Gururow, T. N. *J. Chem. Sci.* **2010**, *122*, 677; (c) Yamada, S.; Sako, N.; Okuda, M.; Hozumi, A. *CrystEngComm*, **2013**, *15*, 199; (d) Aakeröy, C. B.; Schultheiss, N.; Rajbanshi, A.; Desper, J.; Moore, C. *Cryst Growth Des*. **2009**, *9*, 432;

15 (a) Imai, Y.; Inoue, Y.; Nakanishi, I.; Kitaura, K. *Protein Sci*. **2008**, *17*, 1129; (b) Lu, Y.; Wang, Y.; Zhu, W. *Phys. Chem. Chem. Phys*. **2010**, *12*, 4543.

16 (a) de Castro, S. L.; Emery, F. S.; da Silva Júnior, E. N. *Eur. J. Med. Chem.* **2013**, *69*, 678; (b) Ferreira, V. F.; Ferreira, S. B.; da Silva, F. D. C. *Org. Biomol. Chem*. **2010**, *8*, 4793; (c) Lanfranchi, D. A.; -Rodo, E. C.; Bertrand, B.; Huang, H. –H.; Day, L.; Johann, L.; Elhabiri, M.; Becker, K.; Williams, D. L.; -Charvet, E. D. *Org. Biomol. Chem*. **2012**, *10*, 6375; (d) Campos, V. R.; dos Santos, E. A.; Ferreira, V. F.; Montenegro, R. C.; de Souza, M. C. B. V.; -Lotufo, L. V. C.; M. de Moraes, O.; Regufe, A. K. P.; Jordao, A. K.; Pinto, A. C.; Resende, J. A. L. C.; Cunha, A. C. *RSC Advances*, **2012**, *2*, 11438; (e) Tandon, V. K.; Maurya, H. K.; Verma, M. K.; Kumar, R.; Shukla, P. K. *Eur. J. Med. Chem*. **2010**, *45*, 2418.

17 (a) Powis, G. *Pharmacol. Ther*. **1987**, *35*, 57; (b) O'Brien, P. J. *Chem. Biol. Interact*. **1991**, *80*, 1.

18 Frontana, C.; -Mayagoitia, A. V.; Garza, J.; Vargas, R.; Gonzalez, I. *J. Phys. Chem. A*, **2006**, *110*, 9411.

19 (a) Hoover, J. R. E.; Dag, A. R. *J. Am. Chem. Soc.* **1954**, *76*, 4148; (b) Vichkanova, S. A.; Izosimova, S. B.; Adgina, V. V.; Shipulina, L. D. *Rastitel'nye Resursy*, **1979**, *15*, 167; (c) Clark, N. G. *Pestic. Sci.* **1985**, ***16***, 23; (d) Tandon, V. K.; Maurya, H. K.; Tripathi, A.; ShivaKesva, G. B.; Shukla, P. K.; Srivastava, A.; Panda, D. *Eur. J. Med. Chem*., **2009**, ***44***, 1086; (e) Tandon, V. K.; Maurya, H. K.; Yadav, D. B.; Tripathi, A.; Kumar, M.; Shukla, P. K. *Bioorg. Med. Chem. Lett.* **2006**, *16*, 5883.

20 (a) Stagliano, K. W.; Emadi, A. US20040087663A1 (2004); (b) Ganapaty, S.; Thomas, P. S.; Karagianis, G.; Waterman, P. G.; Brun, R. *Phytochemistry*, **2006**, *67*, 1950.

21 Biot, C.; Bauer, H.; Schirmer, R. H.; -Charret, E. D. *J. Med. Chem*. **2004**, *47*, 5972.

22 (a) Pardee,; A. B.; Li, Y. Z.; Li, C. J. *Cancer Drug Targets*, **2002**, *2*, 227; (b) Hazra, B.; Sarma M. D.; Sanyal, U. *J. Chromatogr. B Anal. Technol. Biomed. Life Sci*. **2004**, *812*, 259.

23 (a) Lien, J. –C.; Huang, L. –J.; Wang, J. –P.; Teng, C. –M.; Lee, K. –H.; Kuo, S. –C. *Bioorg. Med. Chem.* **1997**, *5*, 2111; (b) Cunha, S.; Fernandes, L.; Santos, P.; Rocha, Z. N.; Rivelino, R.; Ferrari, J.; Vencato, I.; Lariucci, C.; Nova, Quim. **2010**, *33*, 2108; (c) Pawar, O.; Patekar, A.; Khan, A.; Kathawate, L.; Haram, S.; Markad, G.; Puranik V.; -Gawali, S.S. *J. Mol. Struct.* **2014**, *1059*, 68. (d) Neelgund, G. M.; Budni, M. L.; *Spectrochim. Acta Part A*, **2005**, *61*, 1729.

24 Bittner, S.; Gorohovsky, S.; Paz-Tal (Levi), O.; Becker, J. Y. *Amino Acids*, **2002**, *22*, 71.

25 (a) Pal, S.; Jadhav, M.; Weyhermuller, T.; Patil, Y.; Nethaji, M.; Kasabe, U.; Kathawate, L.; Konkimalla, V. B.;–Gawali, S. S. *J. Mol. Struct*. **2013**, *1049*, 355. (in n-butyl crystal structure also); (b) Knight, J. C.; Tatchell, T.; Fallis, I. A. *Acta Cryst*. **2007**, *E63*, o1226–o1227.

26 Shah, F. A.; Tahir, M. N.; Alia, S.; Kashmiri, M. A. *Acta Cryst.* **2008**, *E64*, o787.

27 Perpete, E. A.; Lambert, C.; Wathelet, V.; Preat, J.; Jacquemin, D. *Spectrochim. Acta A*, **2007**, *68*, 1326.

28 Leyva, E.; Lo´pez, L. I.; -Carrillo, S. E. L.;–Kessler, M. R.; -Rojas, A. M. *J. Fluorine Chem*. **2011**, *132*, 94.

29 Leyva, E.; Sobeck, S. J. S.;–Carrillo, S. E. L.;–Lara, D. A. M. *J. Mol. Struct*. **2014**, *1068*, 1.

30 Win, T.; Bittner, S.*Tetrahedron Lett*. **2005**, *46*, 3229.

31 Ibis, C.; Deniz, N. G. *J. Chem. Sci.*, **2012**, *124*, 657.

32 Zheng, Y.; Ma, K.; Li, H.; Li, J.; He, J.; Sun, X.; Li, R.; Ma, J. *Catal. Lett.* **2009**, *128*, 465.

33 (a) O'Meara, J. A.; Gardee, N.; Jung, M.; Ben, R. N.; Durst, T. *J. Org. Chem.* **1998**, *63*, 3117; (b) Valot, F.; Fache, F.; Jacquot, R.; Spagnol, M.; Lemaire, M. *Tetrahedron Lett*. **1999**, *40*, 3689; (c) Szardening, A. K.; Burkoth, T. S.; Look, G. C.; Campbell, D. A. *J. Org. Chem.* **1996**, *61*, 6720; (d) Chiappe, C.; Pieraccini, D. *Green Chem*. **2003**, *5*, 193.

34 Abreu, F. C. D.; Lopes, A. C. O.; Monte, S. A. D.; Soares, N. A.; Goulart, M. O. F. *J. Electroanalyt. Chem.* **2003**, *560*, 79.

35 Marjolin, A.; Keith, J. A. *ACS Catal.* **2015**, *5*, 1123.

36 (a) Colwell, C. A.; Mccall, M. *Science*, **1945**, *101*, 592. (b) -Ostenhof, O. H. *Science*, **1947**, *105*, 549; (c) Dietz, A. B. Jr., C. C.; Spaubling, *Science*, **1946**, *103*, 399.

37 National Committee for Clinical Laboratory Standards, Performance Standards for Antimicrobial Susceptibility Testing, 8th Informational Supplement. M100 S12, National Committee for Clinical Laboratory Standards, Villanova, Pa, 2002.

38 Soni J. N.; Soman, S. S. *Eur. J. Med. Chem.* **2014**, *75*, 77.

39 Tandon, V. K.; Kumar, S.; Mishra, N. N.; Shukla, P. K. *Eur. J. Med. Chem.* **2012**, *56*, 375.

40 Oxford Diffraction, CrysAlis PRO, Oxford Diffraction Ltd., Yarnton, England, 2009.

41 G.M. Sheldrick, SHELXTL Reference Manual: Version 5.1, Bruker AXS, Madison, WI, 1997.

42 G.M. Sheldrick, SHELXL-97: Program for Crystal Structure Refinement, University of Göttingen, Göttingen, Germany, 1997.

4A.6. Spectra

4A.6.1. IR spectra

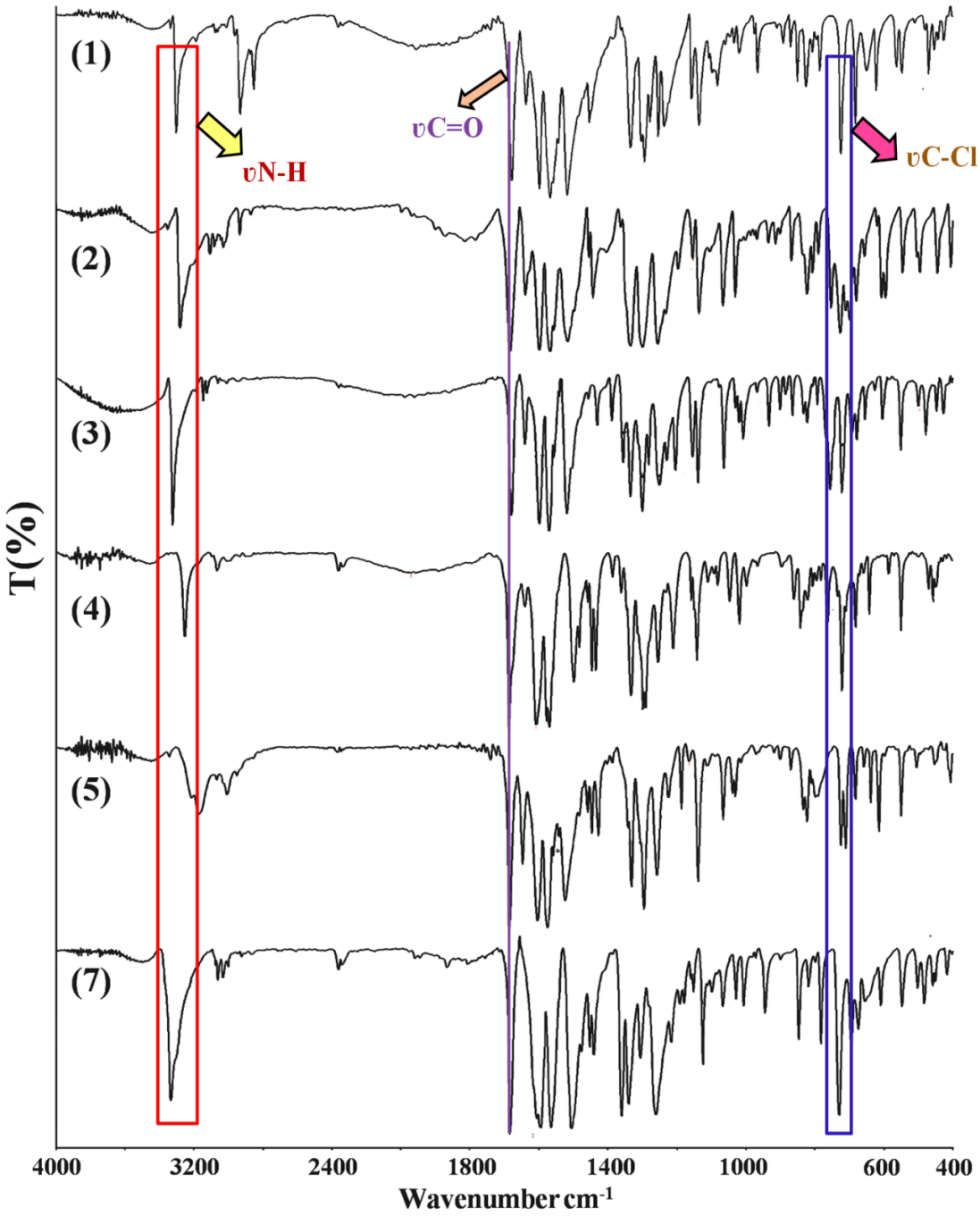

Figure S1. IR spectrum of the amines **1-7**

4A.6.2. NMR spectra

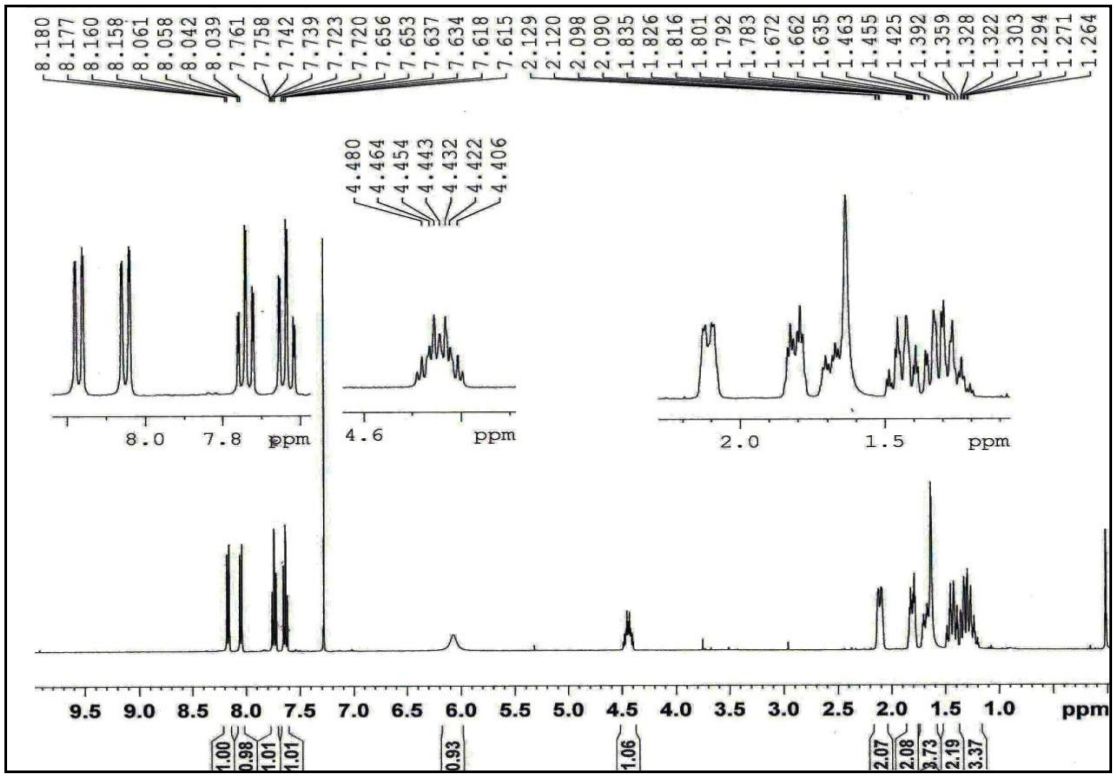

Figure S2. ^{1}H NMR spectrum of compound 1

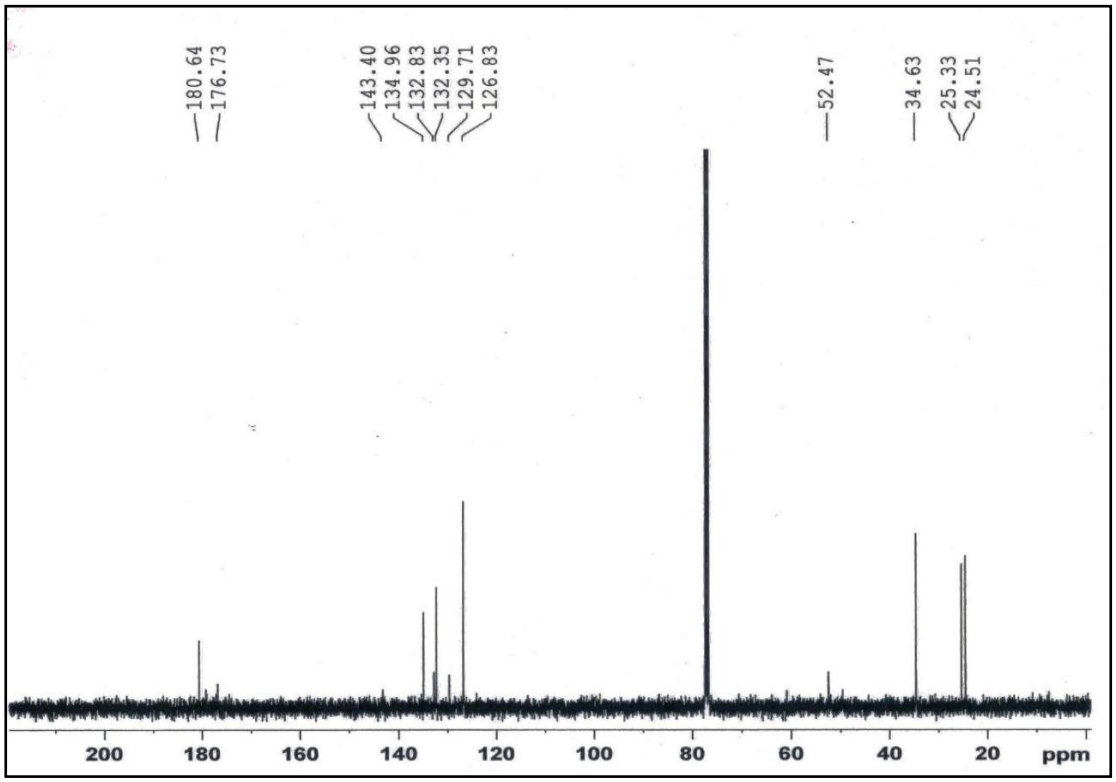

Figure S3. ^{13}C NMR spectrum of compound 1

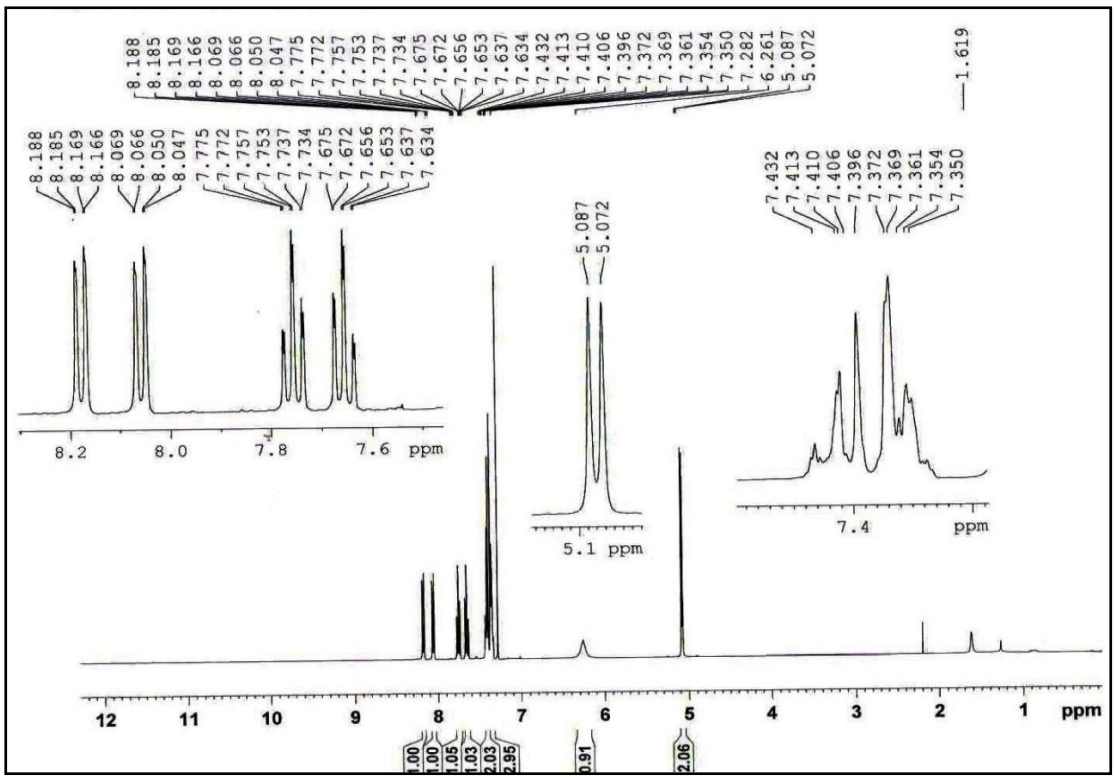

Figure S4. ^{1}H NMR spectrum of compound 2

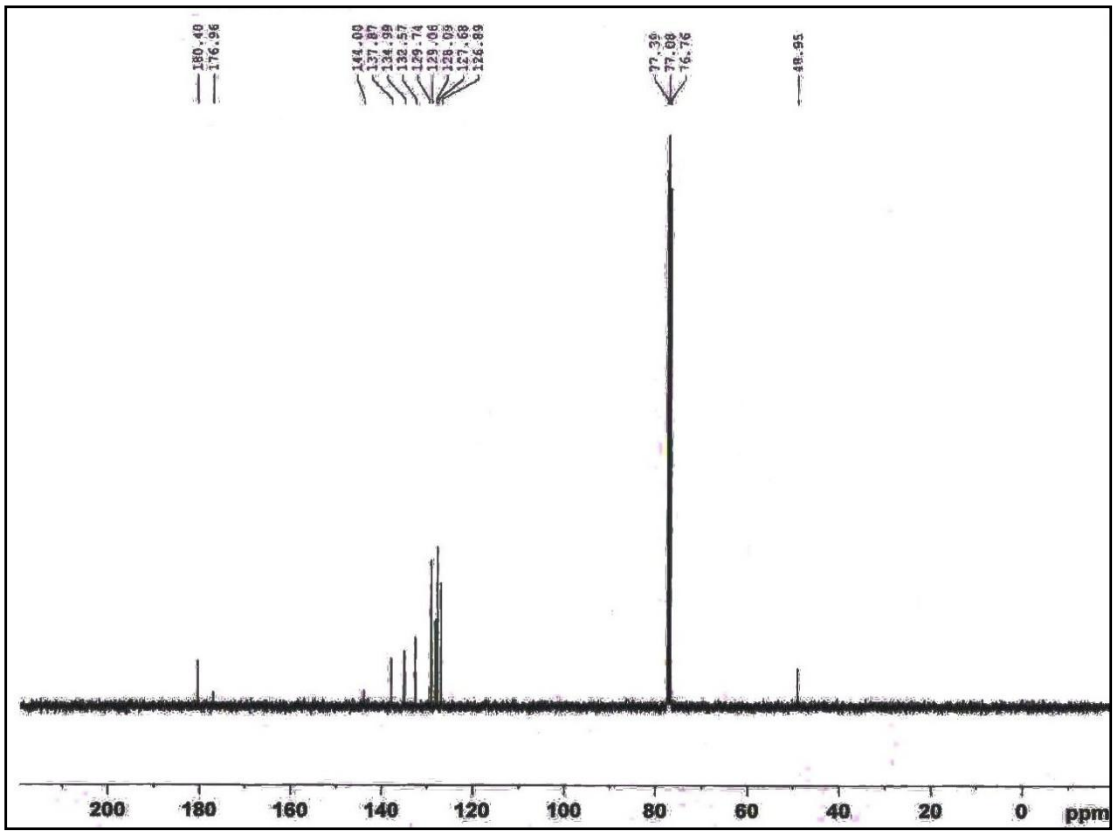

Figure S5. ^{13}C NMR spectrum of compound 2

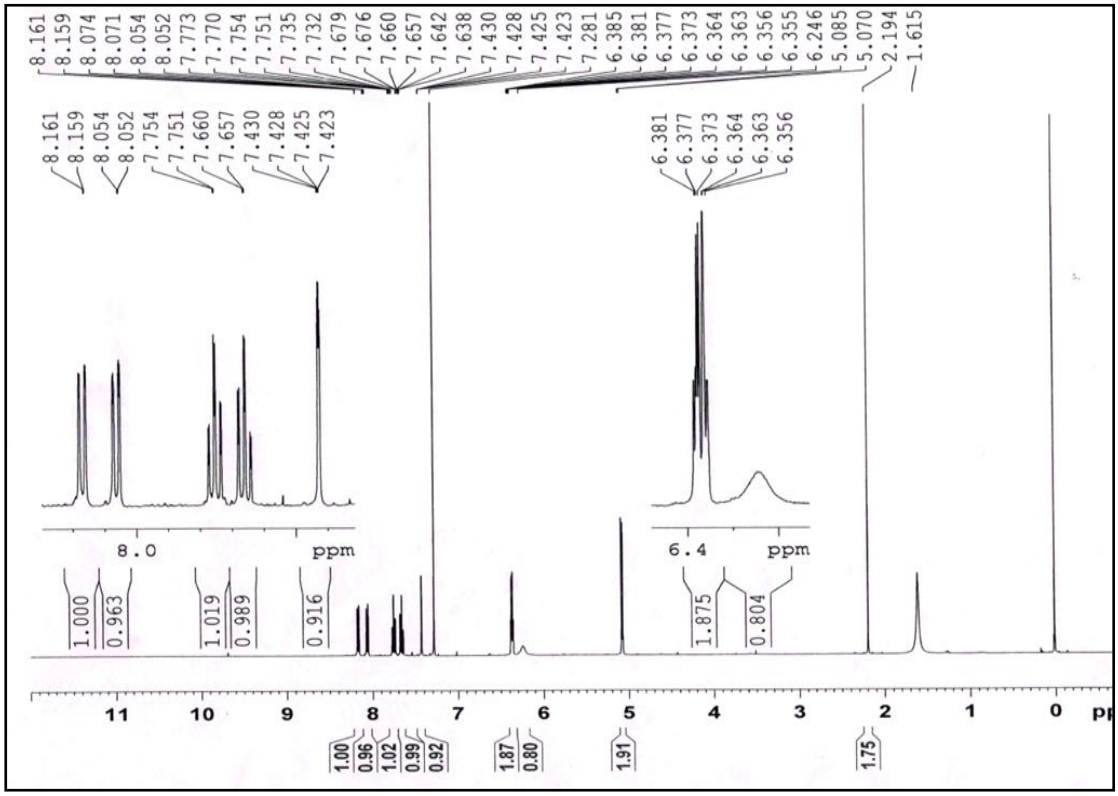

Figure S6. ^{1}H NMR spectrum of compound 3

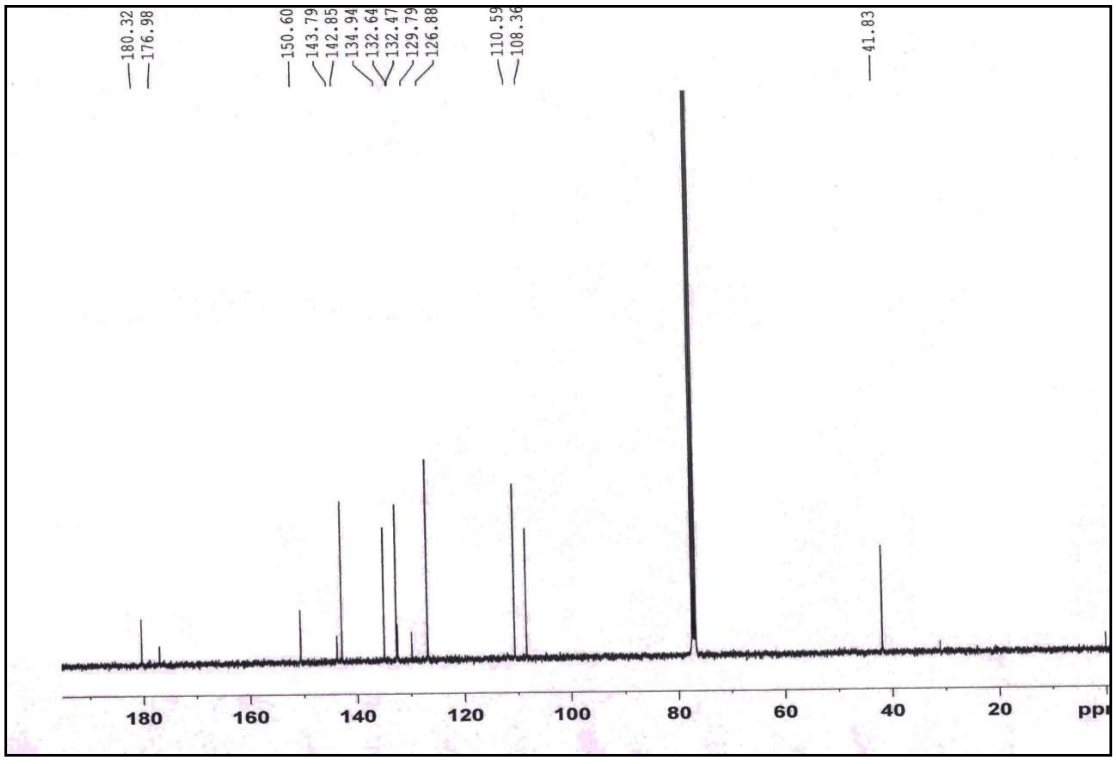

Figure S7. ^{13}C NMR spectrum of compound 3

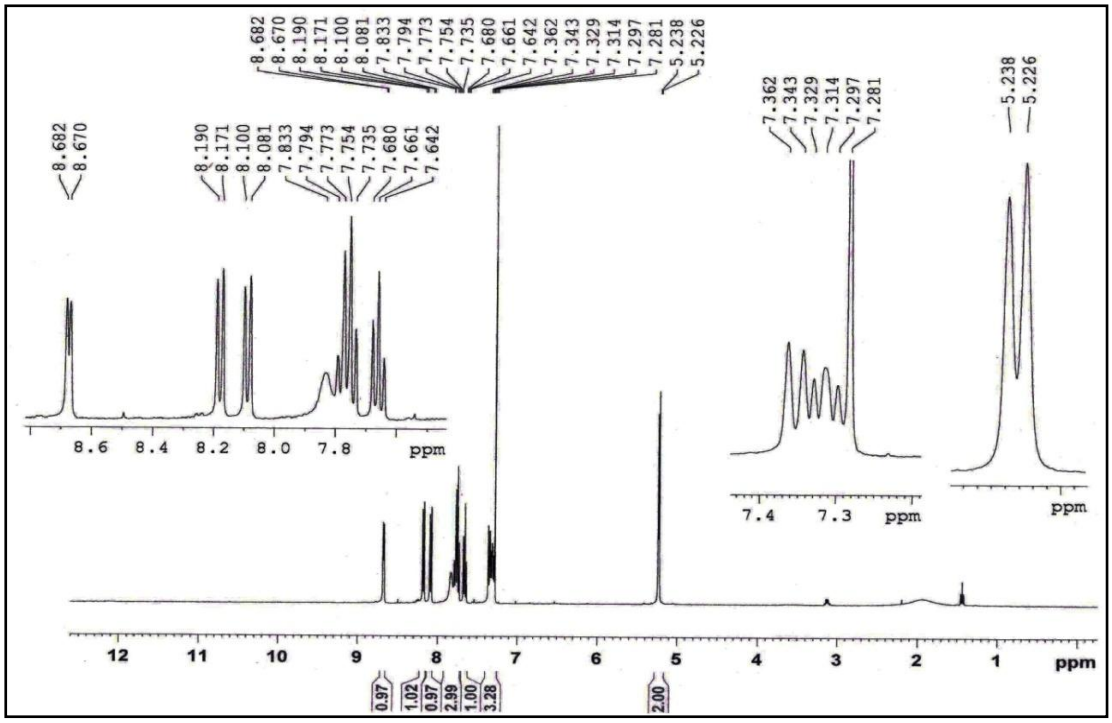

Figure S8. ^{1}H NMR spectrum of compound 4

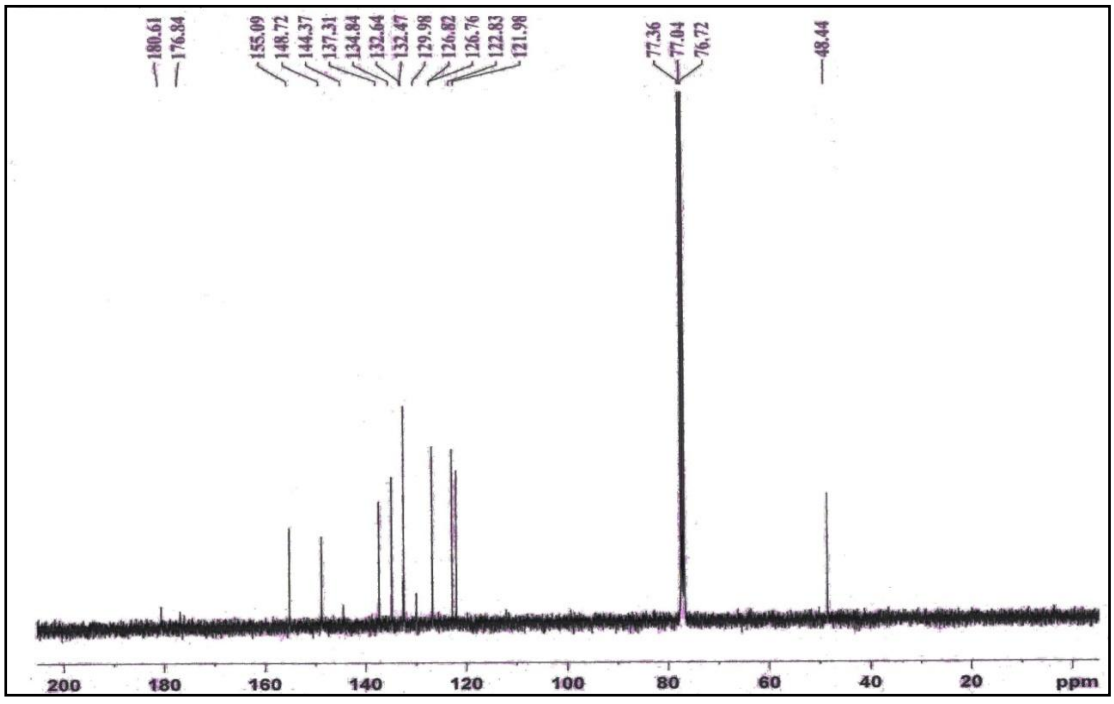

Figure S9. ^{13}C NMR spectrum of compound 4

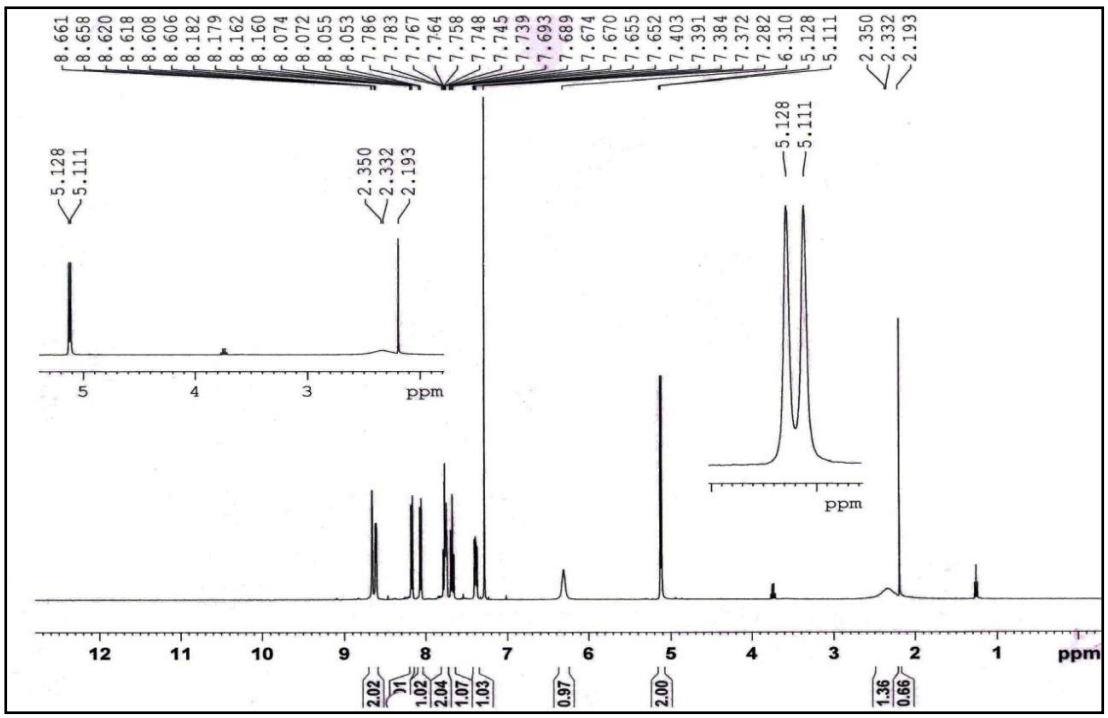

Figure S10. ^{1}H NMR spectrum of compound 5

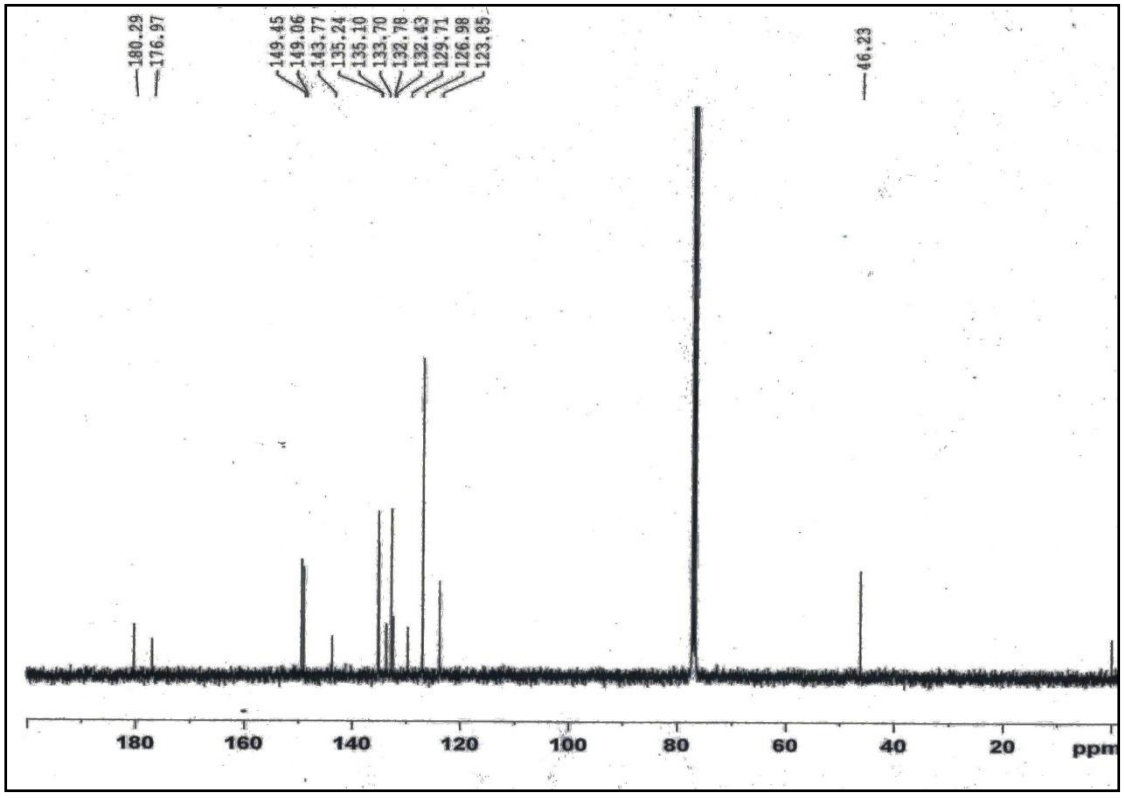

Figure S11. ^{13}C NMR spectrum of compound 5

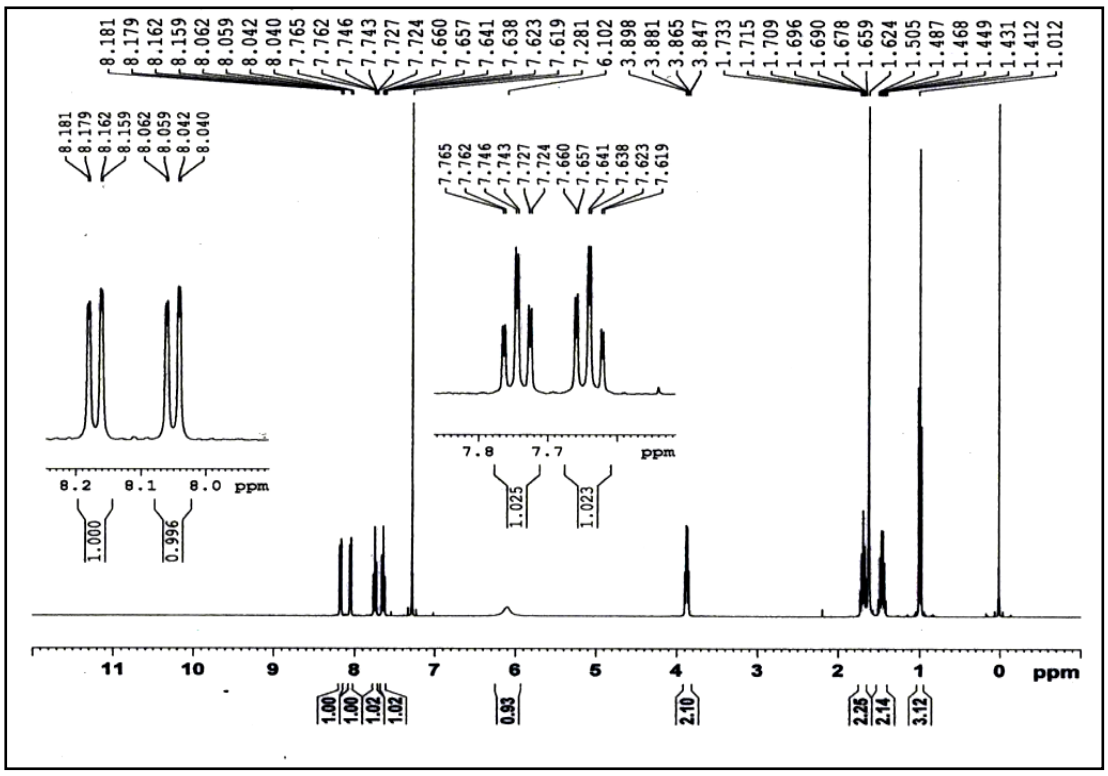

Figure S12. ^{1}H NMR spectrum of compound 6

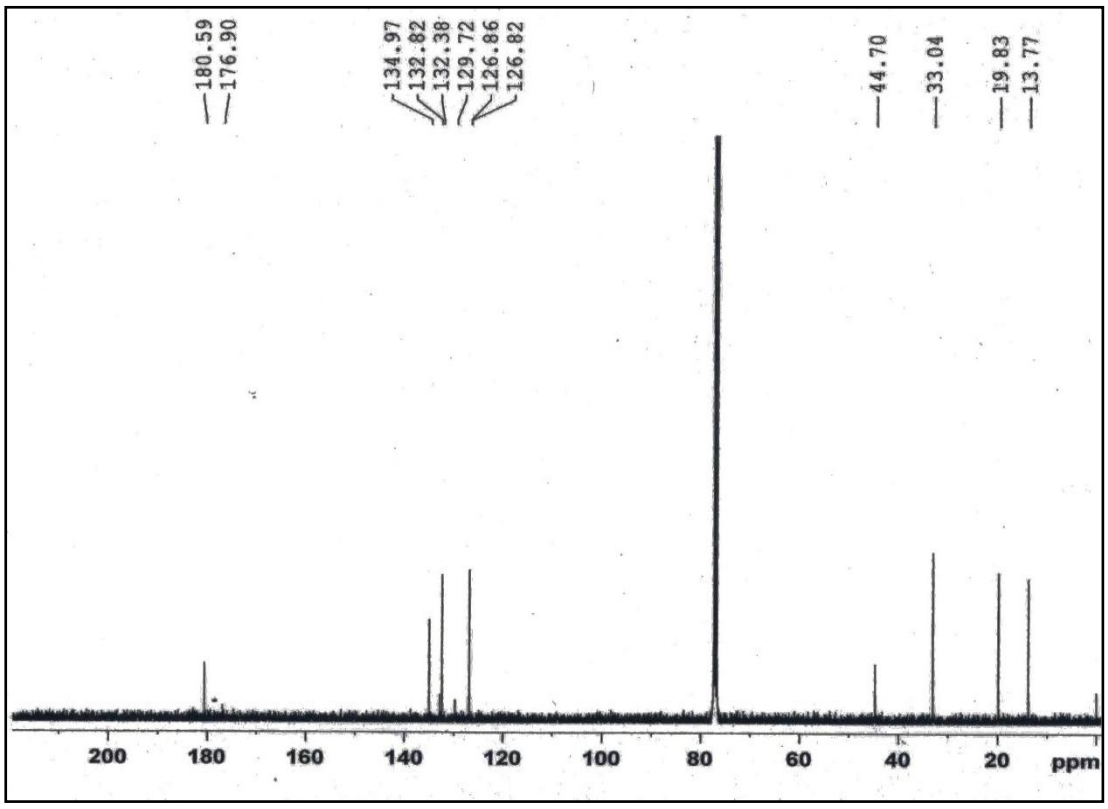

Figure S13. ^{13}C NMR spectrum of compound 6

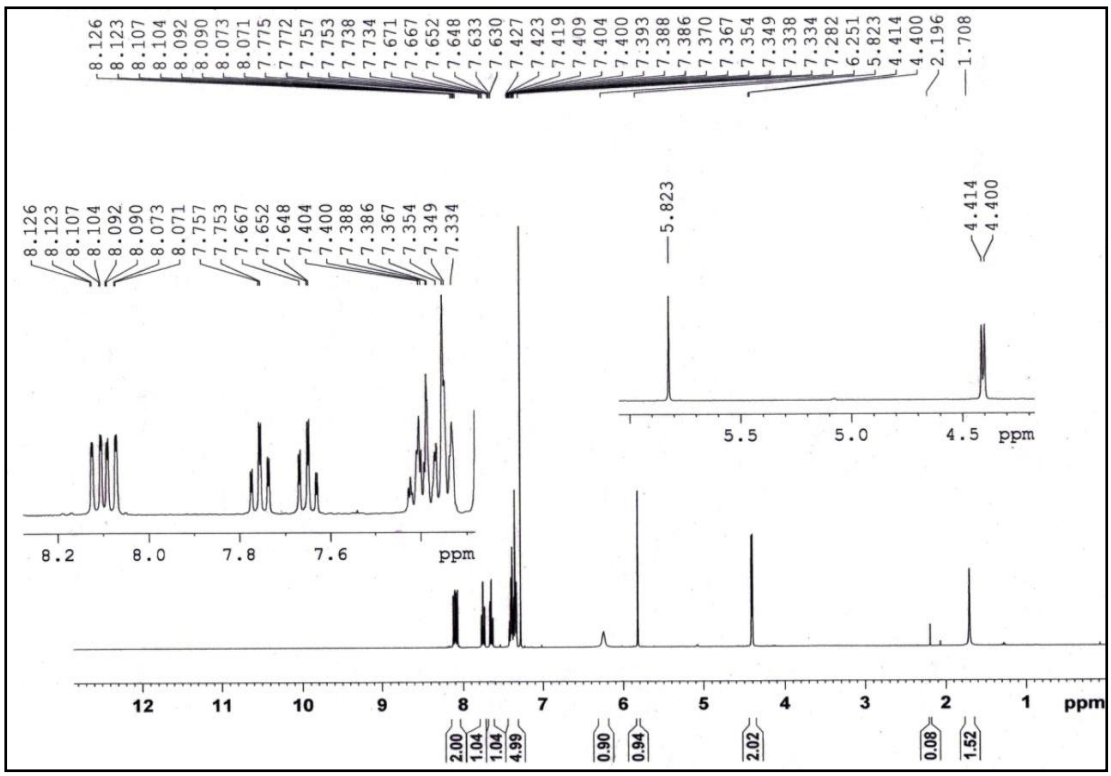

Figure S14. ^{1}H NMR spectrum of compound 7

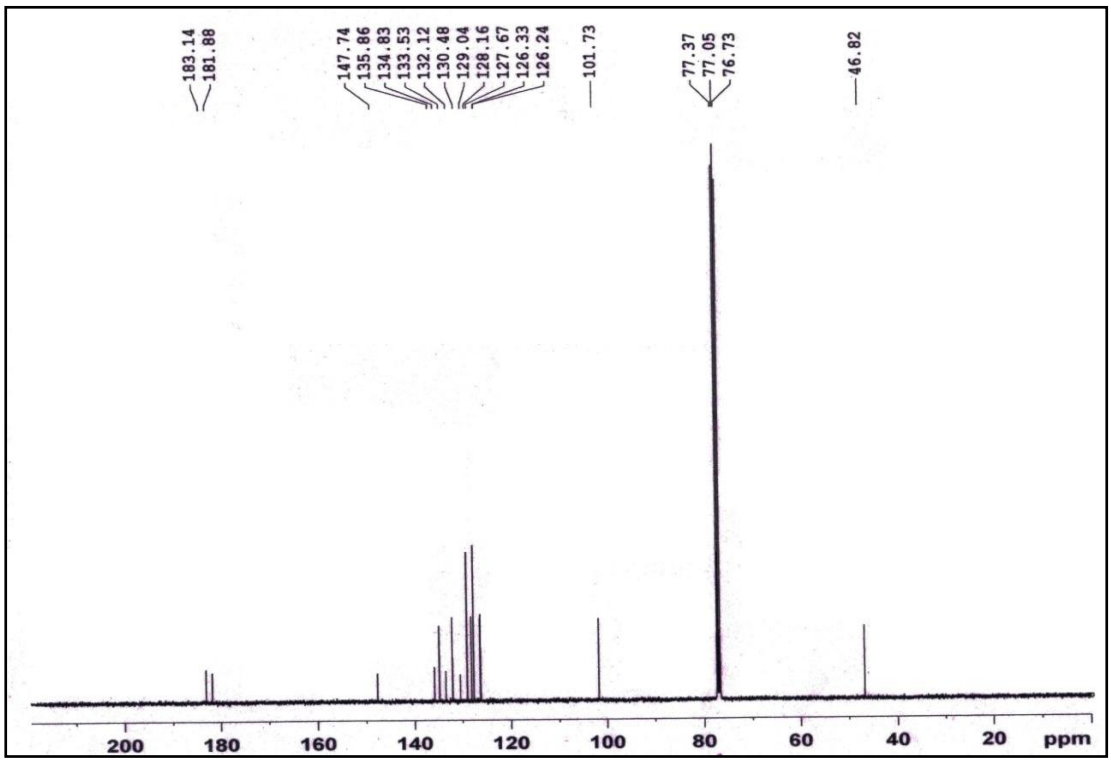

Figure S15. ^{13}C NMR spectrum of compound 7

4A.6.3. GC MS spectra

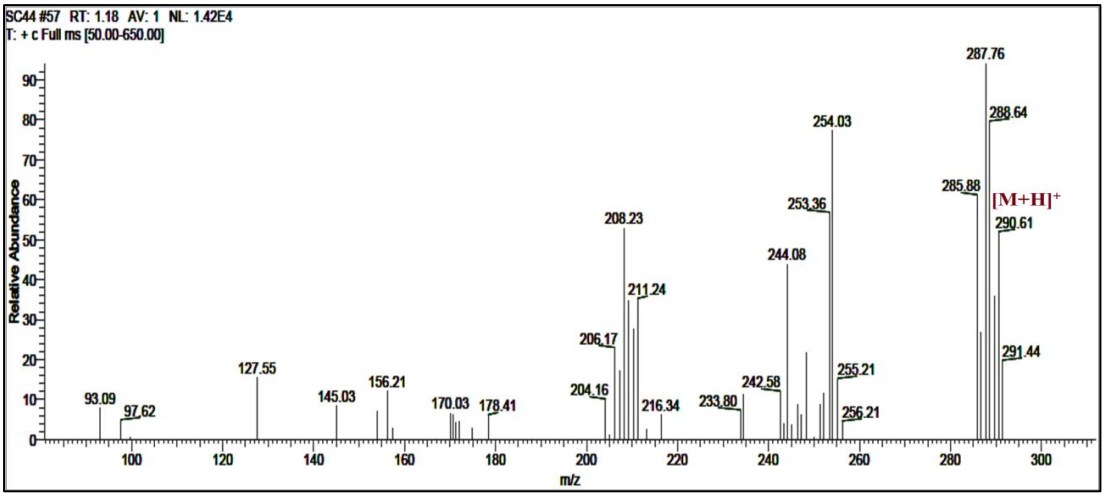

Figure S16. GC MS spectra of compound 1

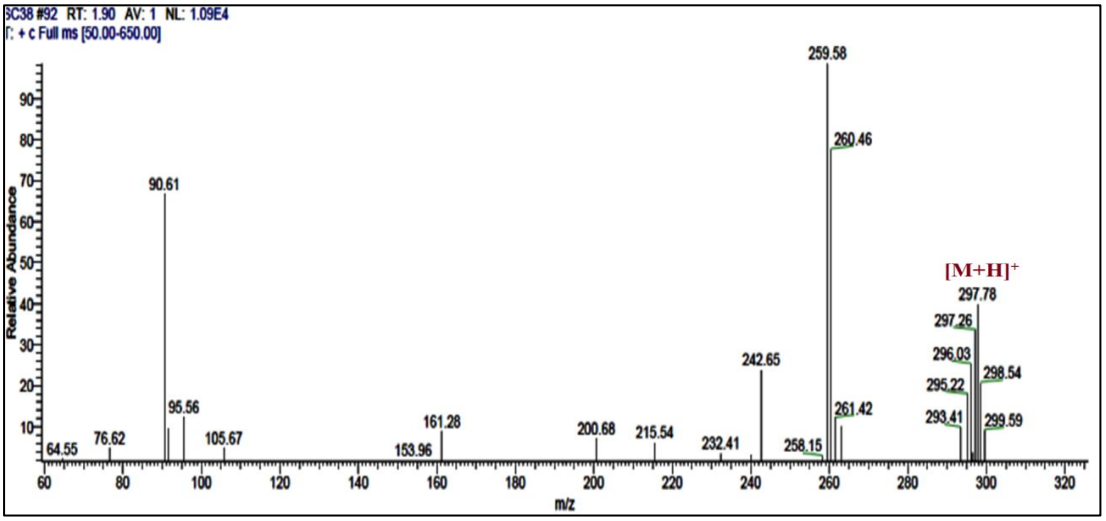

Figure S17. GC MS spectra of compound 2

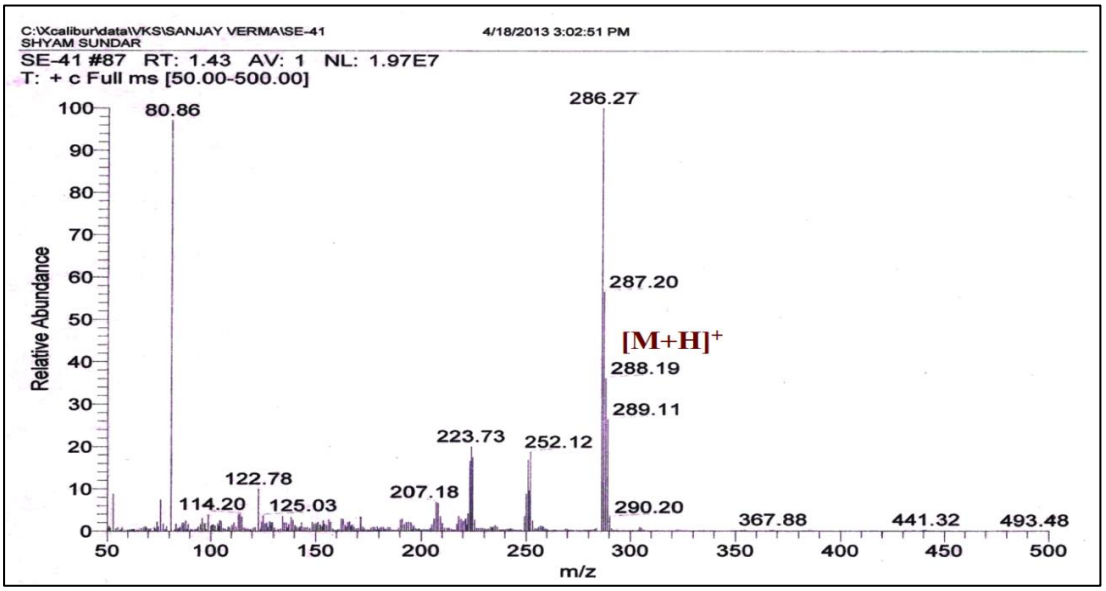

Figure S18. GC MS spectra of compound 3

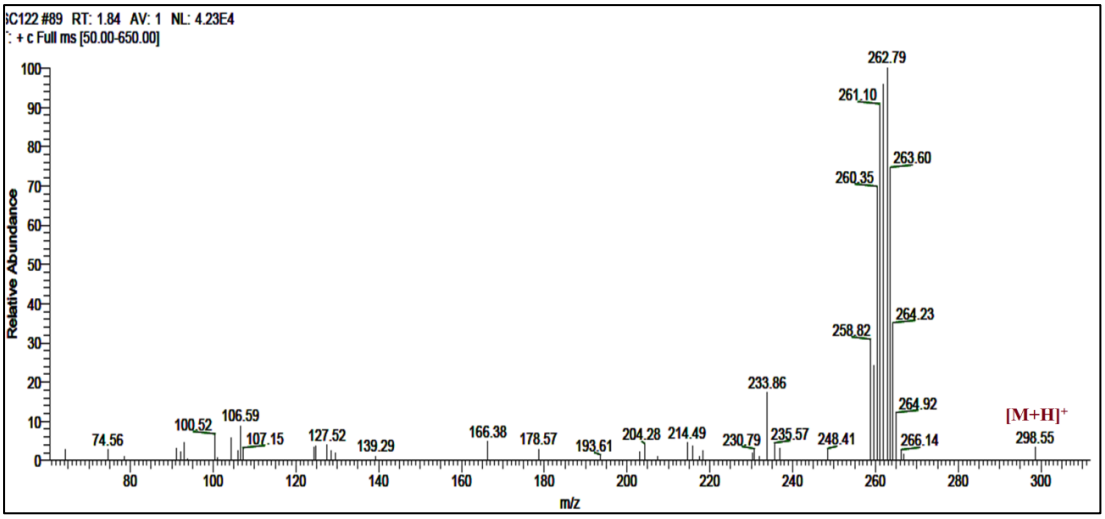

Figure S19. GC MS spectra of compound 4

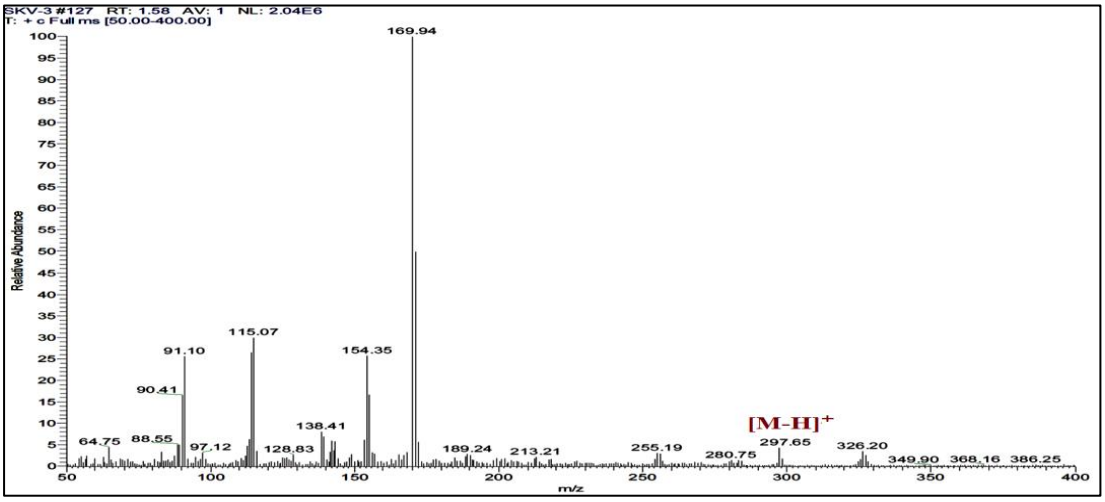

Figure S20. GC MS spectra of compound 5

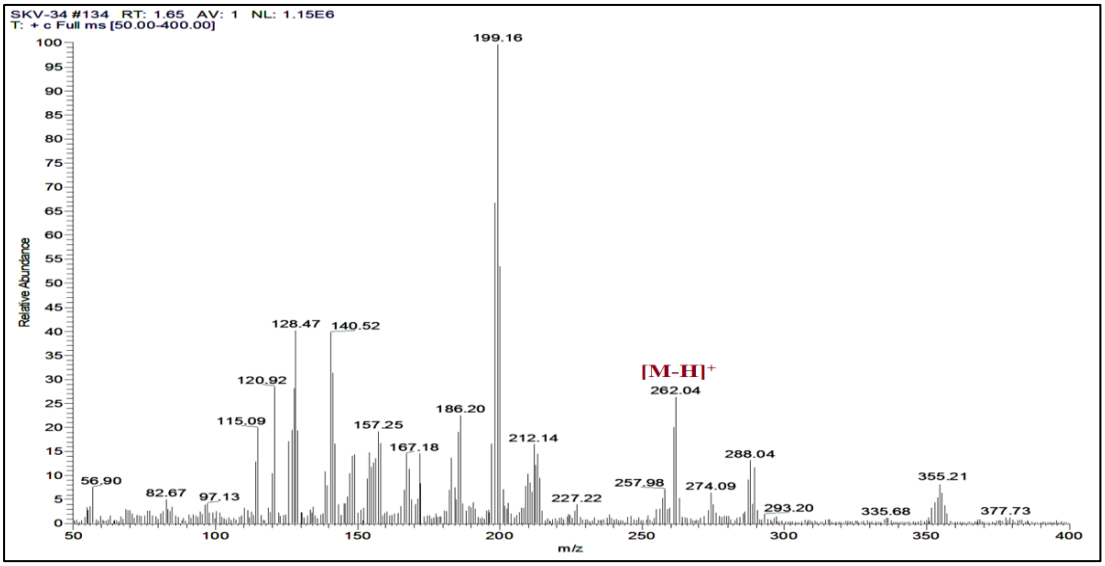

Figure S21. GC MS spectra of compound 6

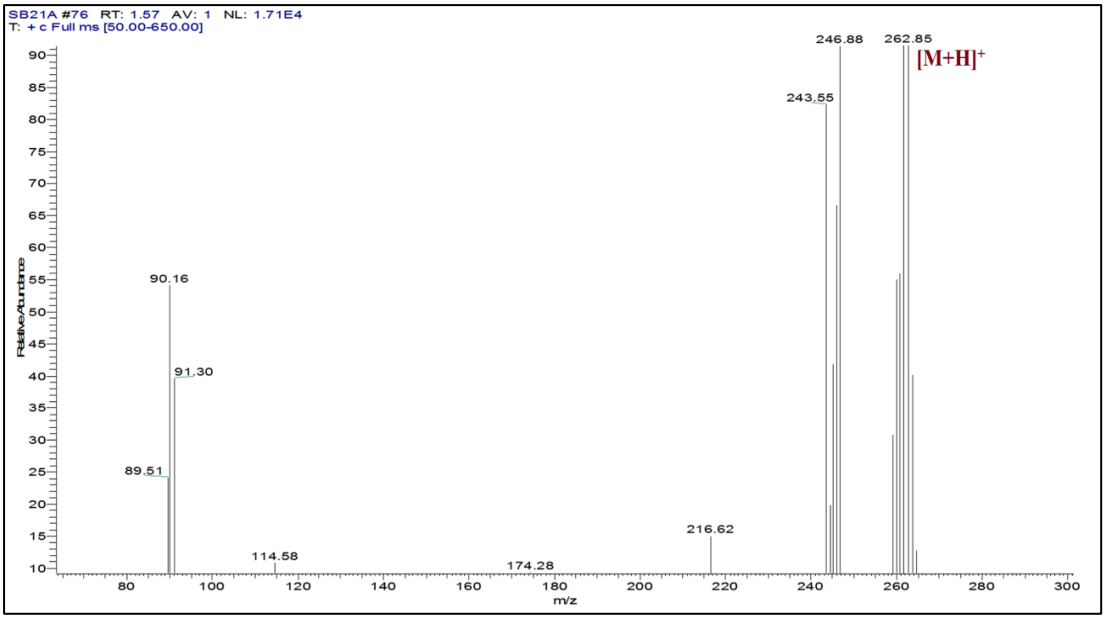

Figure S22. GC MS spectra of compound 7

4A.6.4. Thermogravimmetric data

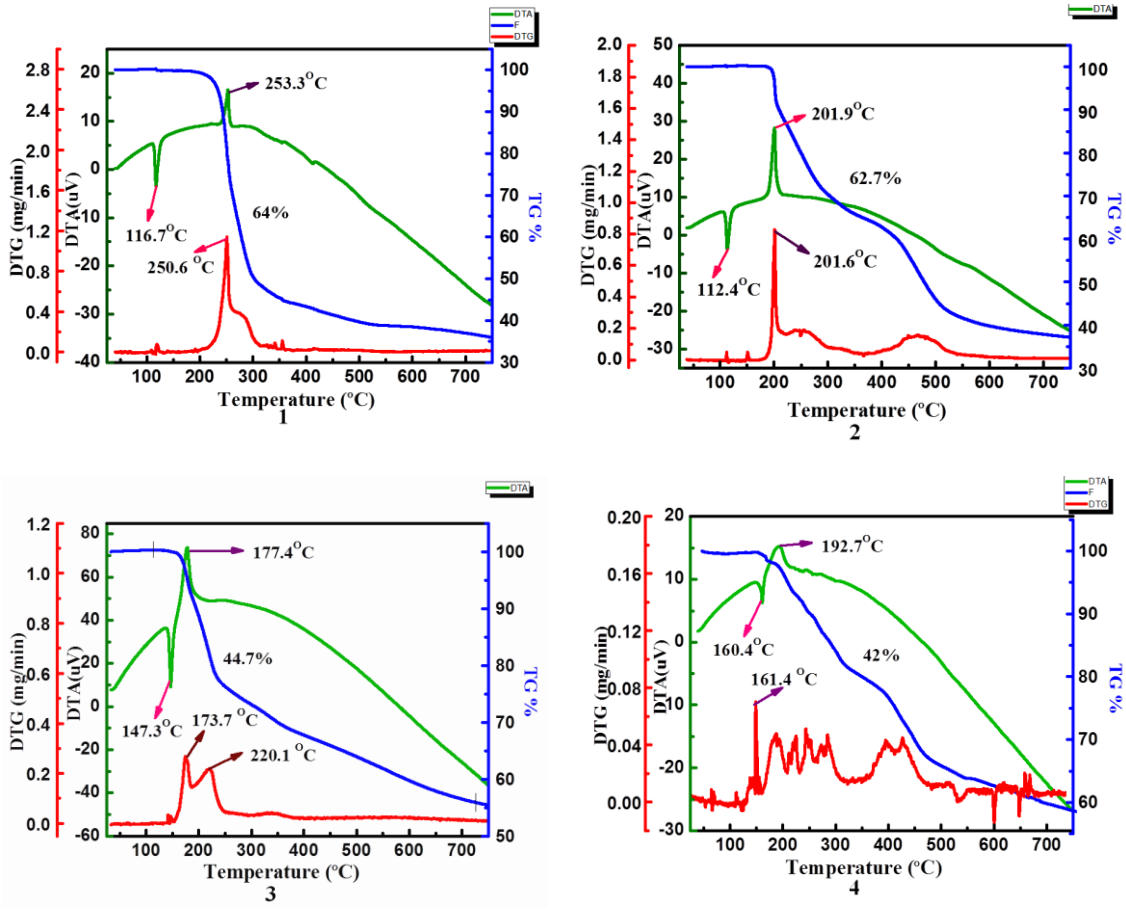

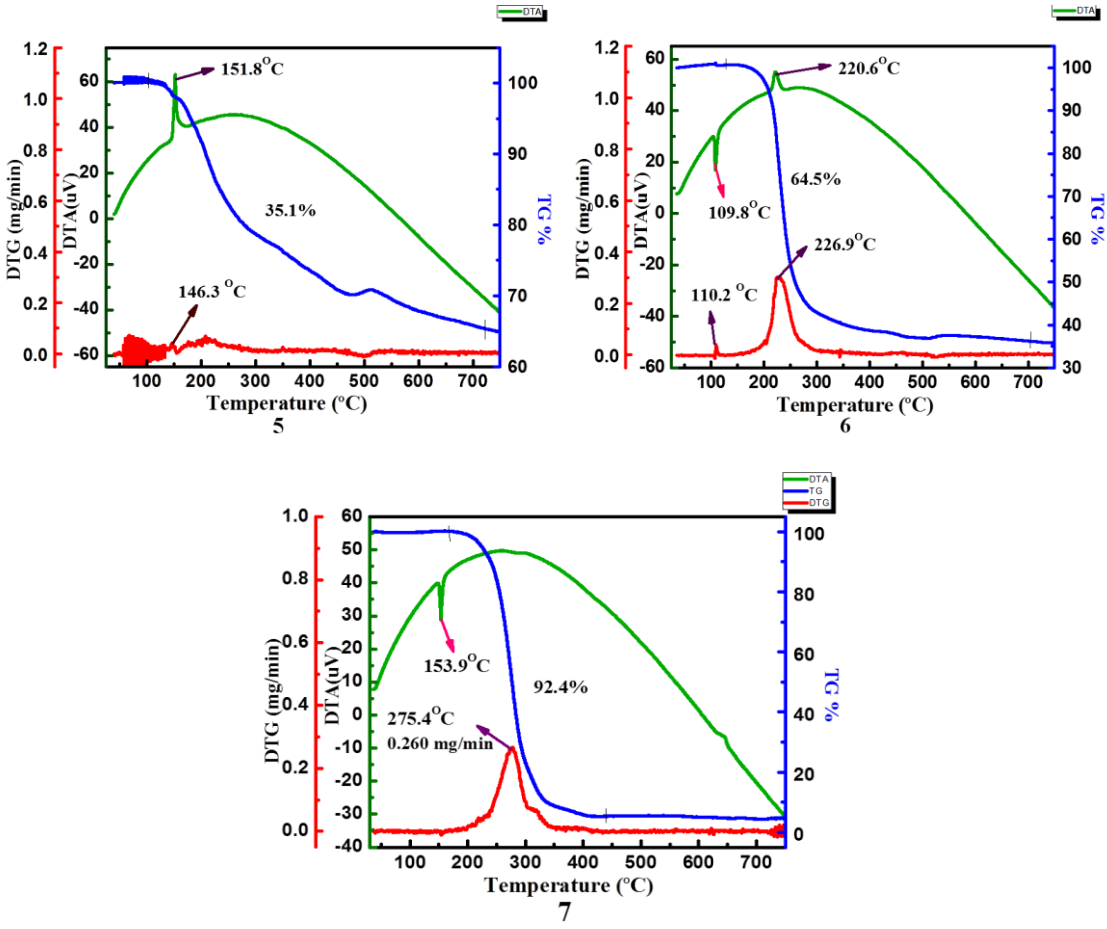

Figure S23. TG/DTA of the compounds 1-7.